Climate variability in the northern Levant from the highly resolved Qadisha record (Lebanon) during the Holocene optimum

Carole Nehme, Sophie Verheyden, Tobias Kluge, Fadi Nader, R. Lawrence Edwards, Hai Cheng, Elisabeth Eiche, Philippe Claeys

Climate variability in the northern Levant from the highly resolved Qadisha record (Lebanon) during the Holocene optimum

Nehme, Carole; Verheyden, Sophie; Kluge, Tobias; Nader, Fadi H.; Edwards, R. Lawrence; Cheng, Hai; Eiche, Elisabeth; Claeys, Philippe

Published in:
Quaternary Research

DOI:
10.1017/qua.2023.24

Publication date:
2024

Climate variability in the northern Levant from highly-resolved Qadisha record (Lebanon) during the Holocene optimum.

Carole Nehme*[1], Sophie Verheyden[2], Tobias Kluge[3], Fadi H. Nader[4], R. Laurence Edwards[5], Hai Cheng[6], Elisabeth Eiche[3], Philippe Claeys[7]

[1] UMR IDEES 6266 CNRS, Université de Rouen-Normandie, France carole.nehme@univ-rouen.fr)
[2]Department of Earth History of Life, Royal Institute of Natural Sciences (RBINS), Brussels, Belgium
[3] Institute of Applied Geosciences, Karlsruhe Institute of Technology, Karlsruhe, Germany
[4]IFP Énergies nouvelles, Direction des Sciences de la Terre et Technologies de l'Environnement, France
[5]Department of Earth and Environmental Sciences, University of Minnesota, Minneapolis, MN 55455, USA
[6]Institute of Global Environmental Change, Xi'an Jiaotong University, Xi'an 710049, China
[7]Analytical Environmental & Geo-Chemistry, Faculty of Science, Vrije Universiteit Brussel, Belgium

Abstract

New stalagmites from Qadisha cave (Lebanon) located at 1720 m asl provides a high-resolution and well-dated record for the northern Mount-Lebanon. The stalagmites grew discontinuously from 9.2 to 5.7 and at 3.5 ka, and they show a tendency from a more negative oxygen-isotope signal at ~9.1 ka to a more positive signal at ~5.8 ka. Such a trend reflects a change from a wetter to a drier climate at high-altitudes. The $\delta^{13}C$ signal shows rapid shifts throughout the record and a decreasing trend towards more negative values in the mid-Holocene, suggesting enhanced soil activity. On the short-term trend, Qadisha stalagmites record rapid dry/wet changes on centennial scales, with a tendency to more rapid dry events towards the mid-Holocene. Such changes are characterized by an overall good agreement between both geochemical proxies and stalagmite growth, and might be affected by the seasonal variations in snow cover. The Qadisha record is in good agreement with other Levantine records, showing more humid conditions from 9 to 7 ka. After 7 ka, a drier climate seems to affect sites at both low- and high-altitude areas. The Qadisha record reflects uniquely mountainous climate particularities compared to other records, specifically the effect of snow cover and its duration, regulating the effective infiltration.

Keywords

Qadisha, Holocene, speleothems, geochemistry, snow cover

1. Introduction

The impact of future climate change in the Eastern Mediterranean (EM), a region already exposed to severe water stress on agriculture and environment, must be better constrained and may be assessed by investigating past climatic variability (Masson-Delmotte et al., 2013). The climate of the Eastern Mediterranean (EM) is influenced by weather systems originating from the North Atlantic Ocean, passing from Europe to the Mediterranean Sea. In the EM region, many records from lake and marine cores (Rohling et al., 2002; Emeis et al., 2003; Jones and Roberts, 2008; Almogi- Labin et al., 2009; Develle et al., 2010) and speleothems (Bar- Matthews et al., 2003; Verheyden et al., 2008; Cheng et al., 2015) have been used to define past climate conditions. Regional paleoclimate records suggest that the region is sensitive to large-amplitude glacial–interglacial changes and climate fluctuations on millennial to decadal timescales (Bar- Matthews et al., 2003; Almogi- Labin et al., 2009; Bar- Matthews and Ayalon, 2011). However, this sensitivity is unequal among regions because of the heterogeneity of the EM climate (Fig. 1) over short distances (Ulbrich et al., 2012). The precipitation distribution shows a high spatio-temporal variability with most of the effective moisture occurring during winter-spring seasons and being concentrated on mountainous regions. Confidently reconstructing this variability requires a dense network of precisely dated and highly resolved palaeoclimate records. Past spatio-temporal climate variability in the EM is still poorly documented due to unevenly distributed records (Burstyn et al., 2019).

In the Levantine region stretching from southern Turkey, Syria, Lebanon, Palestine, Israel to Cyprus, many studies cover the Holocene period, but few are well-dated (Bar-Matthews et al., 2003; Cheng et al., 2015) or record Rapid Climate Changes (RCC). Some are located along the coast at low altitudes like Jeita or Zalmon cave, other records such as Soreq and West Jerusalem caves are located at mid-altitudes (Western flanks of Judean Plateaus). Some lake or marsh records are located in the rain shadow of the Levantine Mountains (e.g. the Dead Sea, the Ammiq marsh in the Beqaa inner plain, the Ghab depression). Among the records covering the Holocene, a few are located in high mountainous areas, such as Mizpe Shelagim cave in Mount (Mt)-Hermon and Incesu cave in the Taurus mountains (Turkey). In the central Levant, Mt-Lebanon (3088 m) is an imposing range facing the moisture coming from the Mediterranean and creates therefore a peculiar local climate system in Lebanon. None of the records spanning the Holocene were retrieved in areas located at high altitude, except for El-Jurd marsh (Chedadi et Khater, 2016) and Yammouneh lake records, which both provide low-resolution (millennial-scale) data. To analyse the effect of mountainous climate and its variability during the Holocene, a reconstruction of past climate variations from highly resolved archives, such as speleothems is needed. These secondary cave deposits (e.g.

stalagmites) are currently considered as the most suitable terrestrial archives for establishing high resolution proxy time-series in paleoclimate research (Genty et al., 2003; Cheng et al., 2012; Fairchild and Baker, 2012).

We report new stalagmite stable-isotope data ($\delta^{13}C$; $\delta^{18}O$) from Qadisha cave (Lebanon) located at 1720 m asl, which provides a high-resolution and well-dated record for the northern Mt-Lebanon covering the time period from 9 to 5 ka. The combined measurements of calcite $\delta^{13}C$ and $\delta^{18}O$ and trace elements enable us to characterise the regional climate trend vs local mountainous effect on high-altitude records. Isotope measurements of fluid inclusions water (δD; $\delta^{18}O_w$) provide insights into the hydrological cycle and allow an estimation of mineral formation temperatures for the Holocene optimum at the high altitude Qadisha Cave.

2. State of the art

During the past decades, several synthesis reports were prepared on paleoclimate studies in the EM (Robinson et al., 2006; Finné et al., 2011; Burstyn et al., 2019), compiling many marine (Rossignol-Strick et al. 1999; Kallel et al. 2000; Emeis et al. 2003; Almogi- Labin et al., 2009) and terrestrial records spanning the Holocene period (Frumkin et al. 2000; Bar-Matthews et al. 2003; Verheyden et al., 2008; Develle et al. 2010, Rowe et al., 2012; Ayalon et al., 2013; Cheng et al., 2015; Gasse et al., 2015; Ünal- İmer et al., 2015; Cheddadi and Khater, 2016; Flohr et al., 2017; Carolin et al., 2019; Sinha et al., 2019; Erkan et al., 2021; Jacobson et al., 2021; Burstyn et al., 2022). Focusing more on the Levantine coast, from the Sinai and Negev desert to the southern flanks of the Taurus Mountains in Turkey, and including Cyprus, studies have revealed a general climatic state of a wet and warm Early Holocene from ~10 to ~6 ka during maximum summer insolation, coeval with the deposition of Sapropel S1. Sapropels are organic-rich layers deposited during periods of increased discharge of the river Nile (Rossignol-Strick et al. 1999; Kallel et al. 2000). This processional time-scale effect results in isotopically lighter sea surface water due to the contribution of the $\delta^{18}O$-depleted Nile influx into the EM sea basin. This isotopic source effect is expressed in Soreq, Peqiin (Bar-Mathews et al., 2003; Bar-Mathews and Ayalon, 2011, Burstyn et al., 2022) and Jeita cave records (Verheyden et al., 2008; Cheng et al., 2015) with more negative oxygen isotope values following the depletion of sea surface $\delta^{18}O$ as resolved from planktonic foraminifera (Grant et al., 2016). In the Southern Taurus mountains, both Dim (Unal-Imer et al., 2015) and Incesu cave records (Erkan et al., 2021) show a trend towards more depleted $\delta^{18}O$ from ~10 to ~8 ka. Although the isotopic composition of the EM source is considered to have a primary effect on the $\delta^{18}O$ signal of the terrestrial records, the isotopic $\delta^{18}O$ depletion is amplified by increased rainfall (Emeis et al., 2003; Almogi-Labin et al., 2009), also leading to more negative $\delta^{18}O$ values. This effect has been invoked for the Early Holocene in some speleothem records (Burstyn et al., 2019) and the Yammouneh polje record (Develle et al., 2010).

The distribution of rainfall and its changes during the Holocene were not-coeval along the Levantine coast. Regional variations in the rainfall amount cause isotopic variations as attested by cave climate monitoring studies (Bar-Matthews et al., 1997; Ayalon et al., 1998; 2004; Nehme et al., 2019). Cave water isotopic values are biased towards the main infiltration period which is the winter-spring season (Nehme et al., 2019; 2020). The isotopic signal of the infiltration water is transferred into the cave calcite. Rapid seasonal, decadal or centennial isotopic variations in speleothems are therefore more likely related to rainfall amount changes (Bar-Matthews et al., 1997; Orland et al., 2014; Nehme et al., 2019) as cave temperature would not vary strongly on seasonal, annual and in deep, less ventilated caves even on decadal scales. The impact of temperature on the calcite $\delta^{18}O$ values is about 0.2‰ per 1°C change (Demeny et al., 2010; Tremaine et al., 2011; Daeron et al., 2019), whereas 200 mm change in the annual rainfall amount could cause a change in the $\delta^{18}O$ of rainfall, and therefore of the infiltrating water by 1‰, as measured at the Soreq cave site by Bar Matthews et al. (2003).

Develle et al., (2010) and Cheng et al., (2015) found contrasting patterns of climate variability between records from northern and southern Levant. Cheng et al. (2015) emphasize an out-of-phase pattern between records from northern Levant relative to the Dead-Sea Basin (DSB). The contrasting pattern of precipitation is likely due to enhanced warm southerly-south-westerly flow which intensifies spring-winter precipitation over northern Levant (Brayshaw et al., 2011). Furthermore, the contrasting north-south precipitation pattern persists on millennial to centennial timescales, linked potentially to an enhanced (weakened) meridional circulation, which results in a wet (dry) northern (southern) Levant (Xoplaki et al., 2004), expressed by a contrasting RCC between Jeita isotopic variations and DSB levels (Cheng et al., 2015).

In parallel to changes in meridional circulation patterns, Cheng et al. (2015) emphasized the relevance of distinct effective infiltration (P-E) effects, enhanced by local factors (topography, vegetation) between the northern and the southern Levant. This interpretation, previously proposed by Develle et al. (2010), focusses on effective rainfall, related to precipitation – evaporation (P-E) in both soil and epikarst that affects water supply to caves (infiltration) and lakes (drainage) and thus explains differences in water balances between sites. Indeed, Develle et al., (2010) stressed on the different timing of rapid climate changes in the northern and the southern Levant.

According to the Jeita cave and Aammiq marsh records (Hajjar et al., 2008), the major shift from humid to general dry conditions occurred around 6 ka, which is different than in the Dead Sea which level was extremely low during the entire Holocene compared to the Late Glacial Maximum (LGM). Migowski et al. (2006) do not exclude those humid conditions relative to modern times prevailed in the DSB during the early-Holocene, but the water balance contrast seen between Yammouneh and DSB records rely on different P-E conditions in both regions. For example, the Yammouneh record (Develle et al., 2010) do not reveal proxy evidence for a drought around 8 ka as observed in Jeita record (Cheng et al., 2015) at lower altitude. More to the South, the 8.2 ka event was pointed out in Soreq record (Bar-Matthews et al., 2003), but was not interpreted as a drought.

Effective infiltration (P-E) also influences proxies related to local soil and epikarst conditions such as $\delta^{13}C$ in carbonates. Such proxies, conditioned by vegetation cover and soil microbial productivity, are additionally influenced by CO_2 degassing and Prior Calcite Precipitation (PCP) related to changing cave drip rates (Fohlmeister et al., 2020). In the EM region, a contrasting pattern of hydroclimate variability between the northern and the southern Levant is exemplified by comparison of the $\delta^{13}C$ profiles of Jeita with Peqiin and Soreq records. Although Jeita and Peqiin cave records show similar $\delta^{13}C$ and $\delta^{18}O$ isotopic trends, a notable heavy excursion in the Soreq $\delta^{13}C$ record from ~10 to ~7 ka presents an opposite trend relative to the Jeita $\delta^{13}C$ curve. This positive Soreq $\delta^{13}C$ event is interpreted to reflect an extremely wet period in the southern Levant partially because of its association with lighter $\delta^{18}O$ values (Bar-Matthews and Ayalon, 2011). Cheng et al., (2015) challenge this interpretation and suggest that the Soreq cave record could reflect drier conditions during the Early Holocene, consistent with low Dead Sea levels, The recent publication of Burstyn et al., (2022) follows the interpretation of Bar-Matthews and Ayalon, (2011) and involves a complex opposite response system of magnetic particle influx to rainfall to demonstrate the coupling between the inflow of magnetic particles (IRM_{flux}) and $\delta^{13}C$ in Soreq speleothems. The contrasting climate between northern and southern Levant are therefore still under debate and the factors such as topography in the local P-E response to the synoptic climate systems still not well constrained mainly due to different interpretations of the $\delta^{13}C$ response to water availability.

3. Current climatic settings of the Levant

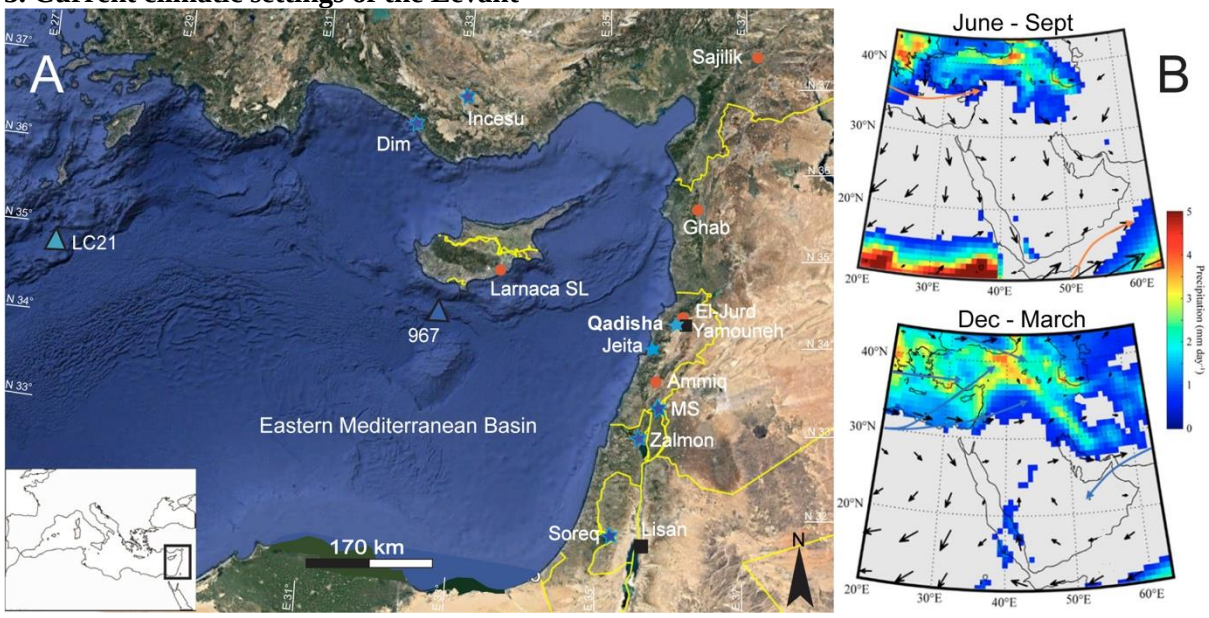

Figure 1. *A-Location of Qadisha Cave (this study) and other paleoclimatic records spanning the Holocene: Lisan lake (Torfstein et al., 2013a, 2013b), Soreq Cave (Bar-Matthews et al., 2003; Burstyn et al., 2022), Zalmon Cave (Keinan et al., 2019)), Peqiin Cave (Bar-Matthews et al., 2003), Mizpe Shelagim (MS) Cave (Ayalon et al., 2013), Ammiq peat record (Hajjar et al., 2008), Jeita Cave (Verheyden et al., 2008; Cheng et al., 2016), Yammouneh Paleolake (Develle et al., 2010), El-Jurd peat record (Chedaddi & Khater, 2016, Ghab core (Zeist & Woldring, 1980; Yasuda et al., 2000), Sagilik peat (Sekeryapan et al., 2020), Incesu Cave (Erkan et al., 2021) Dim Cave (Unal-Imer et al., 2015), Larnaca Salt Lake (Kaniewski et al., 2020), LC21 (Grant et al., 2012), ODP 967 (Emeis et al., 2003; Scrivner et al., 2004). B- Maps showing seasonal precipitation amounts in the wider EM region. Panels at the right illustrate seasonal precipitation amounts from June to September (JJAS) and from December to March (DJFM), respectively. Grey areas indicate regions where the daily precipitation amount is smaller than 0.5 mm. Data retrieved from the ERA-Interim reanalysis dataset (1979 to 2015 CE) (Berrisford et al., 2011)*

Today, the Levant region is mainly influenced by the mid-latitude westerlies, which originate from the Atlantic Ocean, forming a series of sub-synoptic low-pressure systems across the Mediterranean Sea (Gat et al., 2003; Ziv

et al., 2010). In winter, cold air plunging south over the relatively warm Mediterranean enhances cyclogenesis, creating the Cyprus Low (Alpert et al., 2005). Moist air is then driven onshore, generating intense orographic rainfall across Mt-Lebanon, Mt-Hermon and the Syrian mountains in the northern Levant. In summer, the westerly belt is shifted to the north, following the northern shift of the North-African subtropical high pressures, and the region experiences hot and dry conditions with more southward winds. In Lebanon, the annual rainfall varies between 700 and 1000 mm along the coastline and more than 1400 mm in higher mountains. The snow coverage reaches in average 5 months from December to April (Shabaan et al., 2015) in basins located at mid-latitudes (1200-2000 m) and up to 7 months from December to June (Fayad and Gascoin, 2020) in high-altitude basins (>2500 m). As a consequence of the above circulation system, the climate is seasonal with wet winters (November to February) and dry, hot summers (May to October) with a significant influence of snow coverage (up to 75 %) on the water supply budget in karst networks and springs at high-altitudes (Koeninger et al., 2017).

A general West-East gradient in rainfall (amount, isotopic composition) from the Lebanese coastline to the inner Beqaa plain is evident in the published Local Meteoric Waterline (LMWL; Aouad-Rizk et al., 2005) as a consequence of the altitudinal effects related to the Rayleigh distillation processes (Dansgaard, 1964; Rozanski et al., 1993). This gradient is mirrored in the cave stream and dripwater isotopic composition (Nehme et al., 2019) with a clear altitudinal gradient from the coastline to the highest Mt-Lebanon peaks. The North-South Gradient at Mt-Lebanon and to the South is expressed also in the isotopic composition and amount of rainfall. The studies of Aouad-Rizk et al. (2005), Gat et al. (2005), and Saad et al. (2005) showed more positive isotopic rainfall values and a lower rainfall amount towards the south, impacting the water balance (P-E) and effective infiltration in karstic systems along the Levantine coast and mountain chains.

4. Cave site and sample description

Qadisha Cave (34°14'38"N; 36°02'11"E) is located at 1720 m asl in the northern part of Mt-Lebanon (Fig. 1), in the vicinity of the highest peaks (Mt-Makmel) of the mountain chain reaching 3088 m asl. The latter with a North-East - South-West direction faces the East-Mediterranean Basin. The cave develops in Quaternary deposits derived from dolomitised Cretaceous limestone, located in the vicinity of the Qadisha catchment basin (Dubertret, 1975; Nader et al., 2006). The basin is fed by ample snowmelt and has a mean elevation of 2244 m. The duration of snow cover is variable throughout the years and reach 6 to 7 months in the Qadisha water catchment basin (Telesca et al., 2014; Fayad and Gascoin, 2020). The cave is horizontal with more than 1076 m of explored galleries, comprising an upper relict part and lower active part with a permanent spring (discharge rate up to 1 m^3/s) (Edgell, 1997). Qadisha cave, partially transformed in a tourist cave since 1934 (first show cave in Lebanon). It is located nearby the cedar forest of Bsharreh, which is believed to have had a wider forest cover in the past. Today, the Quaternary deposits above the cave, consisting mainly of scree and cemented rock debris, are covered with shrub vegetation (Dubertret, 1975). A previous monitoring study in the cave (Nehme et al., 2019) showed a mean cave-air temperature of 9.0 ± 0.5°C and a pCO_2 concentration of 600 ppmv. Water percolation through the cave persists generally throughout the year. Two speleothems Qad-1 and Qad-2, were retrieved from the upper gallery of the cave, which hosts many active stalagmites.

5. Methods

5.1. ^{230}Th dating

The chronology of Qad-1 and Qad-2 were established by 10 and 9 ^{230}Th dates, respectively (Table 1). Exploratory ^{230}Th dating was performed first at Xi'an Jiaotong University (China) in 2011 and 2014 and the rest was completed at the University of Minnesota (USA) in 2018, by using Thermo-Finnigan Neptune/Neptune plus multi-collector inductively coupled plasma mass spectrometers. The methods are identical in both laboratories (Cheng et al., 2013). Standard chemistry procedures (Edwards et al., 1987) were used to separate uranium and thorium. A triple-spike (^{229}Th-^{233}U-^{236}U) isotope dilution method was used to correct instrumental fractionation and to determine U/Th isotopic ratios and concentrations (Cheng et al., 2013). U and Th isotopes were measured on a MassCom multiplier behind the retarding potential quadrupole in the peak-jumping mode using standard procedures (Cheng et al., 2013). Uncertainties in U/Th isotopic measurements were calculated offline at 2σ, including corrections for blanks, multiplier dark noise, abundance sensitivity, and contents of the same nuclides in spike solution. Corrected ^{230}Th ages assume an initial ^{230}Th/^{232}Th atomic ratio of 4.4 ± 2.2 x10^{-6}, the values for a material at secular equilibrium with a bulk earth ^{232}Th/^{238}U value of 3.8 (Cheng et al., 2013).

Table 1. *^{230}Th dating results of stalagmites Qad-stm1 and Qad-stm2. The error is given as 2se. U decay constants: l^{238} = 1.55125x10-10 (Jaffey et al., 1971) and l^{234} = 2.82206x10-6 (Cheng et al., 2013). Th decay constant: l^{230} = 9.1705x10-6 (Cheng et al., 2013). *$d^{234}U$ = ([$^{234}U/^{238}U$] activity –1)x1000. ** $d^{234}U$ initial was calculated based on ^{230}Th age (T), i.e., $d^{234}Uinitial = d^{234}Umeasured$ x el234xT. Corrected ^{230}Th ages assume the initial $^{230}Th/^{232}Th$ atomic ratio of 4.4 ±2.2 x10-6. Those are the values for a material at secular equilibrium, with the bulk earth $^{232}Th/^{238}U$ value of 3.8. The errors are arbitrarily assumed to be 50%. ***CE stands for "Contemporaneous Era". Ages are defined as the year before 1950 A.D. *age considered as outlier*

Sample Number	depth (mm)	^{238}U (ppb)	^{232}Th (ppt)	^{230}Th / ^{232}Th (atomic x10^{-6})	$\delta^{234}U$* (measured)	^{230}Th / ^{238}U (activity)	^{230}Th Age (a) (uncorrected)	^{230}Th Age (a) (corrected)	$\delta^{234}U_{initial}$** (corrected)	230Th Age (yr CE)*** (corrected)
Qad-stm1-0	2	435,0 ±1,0	3591 ±72	85 ±2	353,7 ±2,2	0,0426 ±0,0002	3848 ±19	**3307 ±127**	357 ±2	**3247 ±127**
Qad-stm1-8	7	606,5 ±0,6	132 ±3	5739 ±140	442,4 ±1,5	0,0756 ±0,0003	5853 ±28	**5848 ±28**	450 ±1	**5780 ±28**
Qad-stm1-7	26	575,7 ±0,9	97 ±3	7502 ±240	444,3 ±2,2	0,0764 ±0,0004	5914 ±30	**5911 ±30**	452 ±2	**5843 ±30**
Qad-stm1-6	46	615,3 ±1,0	122 ±3	6432 ±183	450,6 ±2,0	0,0774 ±0,0004	5966 ±29	**5962 ±29**	458 ±2	**5894 ±29**
Qad-stm1-5	65	665,4 ±0,7	361 ±8	2329 ±50	445,7 ±1,7	0,0767 ±0,0003	5929 ±24	**5918 ±25**	453 ±2	**5850 ±25**
Qad-stm1-4	77	535,7 ±1,0	466 ±10	1472 ±31	437,3 ±2,7	0,0777 ±0,0004	6045 ±33	**6028 ±35**	445 ±3	**5960 ±35**
Qad-stm1-3	96	572,6 ±0,6	352 ±7	2126 ±46	432,1 ±1,5	0,0792 ±0,0003	6185 ±28	**6173 ±29**	440 ±2	**6105 ±29**
Qad-stm1-2	101	546,2 ±0,6	66 ±2	11419 ±389	441,9 ±1,8	0,0840 ±0,0003	6528 ±25	**6525 ±25**	450 ±2	**6457 ±25**
Qad-stm1-1	115	643,7 ±1,1	1156 ±23	792 ±16	433,5 ±2,2	0,0863 ±0,0003	6748 ±28	**6711 ±38**	442 ±2	**6643 ±38**
Qad-stm1-00*	128	639,0 ±2,0	978 ±20	902 ±18	428,1 ±2,6	0,0838 ±0,0003	6573 ±24	**6542 ±32**	436 ±3	**6482 ±32**
Qad-Stm2-5	6	558,6 ±1,5	194 ±4	45 ±3	303,3 ±2,1	0,0009 ±0,0001	79 ±5	**71 ±7**	303 ±2	**5 ±7**
Qad-stm2-4	13	297,6 ±0,3	193 ±4	2309 ±51	397,4 ±1,7	0,0907 ±0,0004	7294 ±36	**7281 ±37**	406 ±2	**7213 ±37**
Qad-stm2-3	25	621,7 ±0,6	316 ±6	3161 ±65	406,2 ±1,4	0,0973 ±0,0002	7794 ±22	**7783 ±23**	415 ±1	**7715 ±23**
Quad 2-8.2	28.2	351,8 ±0,3	255 ±6	2284 ±50	423,4 ±1,6	0,1003 ±0,0004	7937 ±38	**7922 ±39**	433 ±2	**7851 ±39**
Qad-stm2-2	30	336,4 ±0,5	87 ±2	6980 ±178	457,5 ±2,1	0,1093 ±0,0004	8466 ±32	**8461 ±33**	469 ±2	**8393 ±33**
Qad stm2-8.6	36	367,1 ±0,3	284 ±6	2422 ±52	483,2 ±1,6	0,1138 ±0,0004	8667 ±35	**8652 ±36**	495 ±2	**8581 ±36**
Qad-stm2-8	49	499,2 ±0,7	62 ±2	15661 ±580	481,2 ±2,2	0,1186 ±0,0004	9062 ±35	**9060 ±35**	494 ±2	**8992 ±35**
Qad-stm2-7	67	582,4 ±0,8	188 ±4	6121 ±144	484,8 ±2,1	0,1200 ±0,0004	9153 ±34	**9147 ±34**	497 ±2	**9079 ±34**
Qad-stm2-6	80	566,7 ±0,8	379 ±8	2970 ±63	489,1 ±2,1	0,1206 ±0,0004	9167 ±34	**9154 ±35**	502 ±2	**9086 ±35**
Qad-Stm2-1	106	545,4 ±0,9	207 ±4	5220 ±106	472,7 ±1,4	0,1199 ±0,0002	9218 ±20	**9211 ±21**	485 ±1	**9145 ±21**

5.2. Calcite and water stable-isotopes measurements

Samples for stable isotopic analyses were taken along the growth axis of Qad-1 and Qad-2 stalagmites (Fig 2) for $\delta^{13}C$ and $\delta^{18}O$ measurements. Overall, 230 samples were measured in both stalagmites. Samples were drilled along the stalagmite growth axis at 2.5 mm resolution using a Merchantek Micromill mounted on a Leica microscope, with a 0.3 mm resolution for specific parts. Between every sample, the drill bit and sampling surface were cleaned with compressed air. The samples were analysed using a Nu Carb carbonate device coupled to a Nu Perspective mass spectrometer (MS) at the Vrije Universiteit Brussel, Belgium. Parts of the samples were measured at the Laboratory for Environmental and Raw Material Analysis (LERA) at Karlsruhe institute of Technology (KIT), Germany, using a Thermo Gasbench II connected to a DELTA V IRMS in continuous flow mode. All $\delta^{18}O$ and $\delta^{13}C$ values are calibrated against Vienna Pee-Dee Belemnite (V-PDB) and are reported in permil (‰). Analytical uncertainties were better than 0.1 ‰ (1σ) for oxygen and 0.05 ‰ (1σ) for carbon on both instruments. Percolation and stream waters as well as recent calcite samples underneath active drip water were collected previously from Qadisha cave in 2011 and 2014 (Nehme et al., 2019).

5.3. Trace element data

Elemental abundances were determined by laser ablation (LA)-ICP-MS, at the Institute for Geosciences, Johannes Gutenberg University Mainz, Germany, using an ESI NWR193 ArF excimer LA system equipped with the TwoVol^2 ablation cell, operating at 193 nm wavelength, coupled to an Agilent 7500ce quadrupole ICP-MS. Ablation was performed in line scan mode and surfaces were pre-ablated prior to each line scan to prevent potential surface contamination. Line scans were performed at a scan speed of 10 µm/s, using a spot size of 110 µm and a laser repetition rate of 10 Hz. Laser energy on the samples was about 3 J/cm^2. Measured ion intensities were monitored in time-resolved mode and background intensities were measured for 15s. Synthetic glass NIST SRM 612 was used to calibrate element concentrations applying the preferred values given in the GeoReM database (; Jochum et al., 2005; 2012). Quality control materials (QCMs) (USGS MACS-3 and USGS BCR-2G) were used to monitor the accuracy and precision of the LA-ICP-MS analysis and calibration strategy. Raw data were processed using TERMITE (Mischel et al., 2017), an R script for data reduction. ^{43}Ca was used as an internal standard and applied at a sample Ca concentration of 390,000 µg/g and the values reported in the GeoReM data base for the QCMs. Element concentrations determined for the QCMs had a precision of <0.02% (1σ).

5.4. Fluid inclusions stable-isotope (H-O) analyses

Five calcite samples, from three levels in Qad-2 stalagmite were measured using a custom-built extraction line connected to a Picarro L2130i analyzer using cavity ring down spectroscopy (WSCRDS). This technique allows to simultaneously measure hydrogen and oxygen isotopes for minute water amounts released from calcite. The extraction line follows the design of Affolter et al. (2014) and is described in detail in Weissbach et al. (2022). In brief, the calcite samples were hydraulically crushed, and the released fluid inclusion water instantly vaporized in the heated extraction system and transferred to the analyser. Reference water injections with known $\delta^{18}O$ and δD values were used for calibration and quality control. Glass capillaries (µl size) were used for high-precision water amount calibration and isotopic control. The precision of fluid inclusion water analyses is dependent on the released water amount and is 0.5 ‰ for $\delta^{18}O$ and 1.2 ‰ for δ^2H, if fluid water amounts are >0.2 µl and reaches 0.1-0.3 ‰ for $\delta^{18}O$ and 0.2-0.7 ‰ for δ^2H for fluid water amounts >1 µl (Weissbach et al., 2022).

6. Results

6.1. Petrography and chronology

Both samples of 11 and 13 cm each display along their growth axis a translucent to whitish calcite with a columnar fabric observed over most sections. Both stalagmites are highly laminated. With the aid of a camera mounted on a Leica Microscope, images of laminae were taken at several depths and the thickness of each was measured. Layer thickness of laminae varied between 60 µm to 280 µm. The laminae growth is irregular and alternates between thin (60 -70 µm) to thick laminae (200-280 µm).

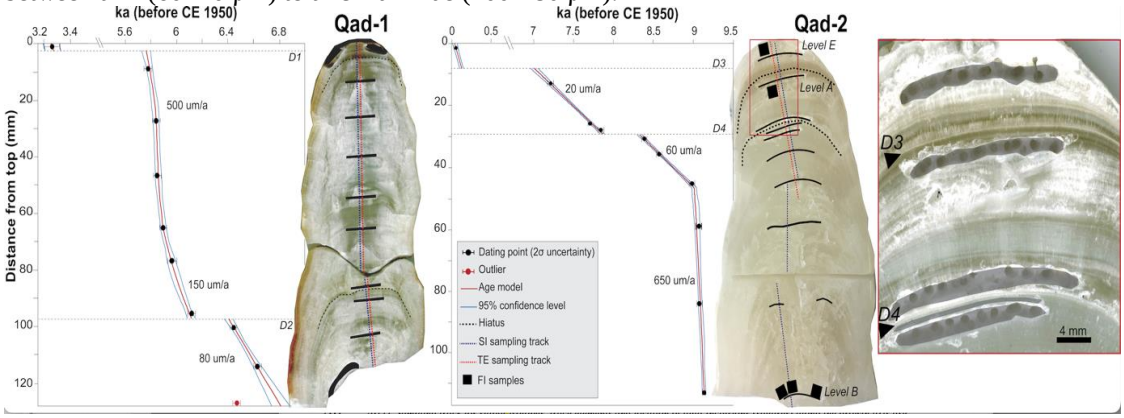

Figure 2. *Age model of both Qadisha-1 (Qad-1) and Qadisha-2 (Qad-2) stalagmites using StalAge (Scholz and Hofmann, 2011). Sampling track for stable-isotopes, trace elements and location of fluid Inclusions (squares) along the growth axis are shown on each stalagmite. Red rectangle in the upper part of Qad-2 stalagmite shows a high-resolution image of the discontinuities D3 and D4 along the growth axis.*

A total of 19 Uranium/Thorium ages were obtained from stalagmites Qad-1 and Qad-2 (Table 1). The age distribution based on the StalAge model (Scholz and Hofmann, 2011) indicates that the stalagmite Qad-1 grew from ca. 6.643 ± 0.038 to 3.247 ± 0.127 ka including two discontinuities (Fig. 2). The first discontinuity D1 ranges from 3.247 to 5.787 ka (extrapolated ages) and D2 covers a shorter period from 6.108 to 6.408 ka (extrapolated ages). Qad-2 grew from 9.145 ± 0.021 to 0.005 ± 0.007 ka including two discontinuities: D3 (0.005 to 7.016 ka) and D4 (7.844 to 8.326 ka). The age model of Qad-1 was constructed with 8 ages, and one age (Qad-stm1-00) considered as an outlier. The latter is sampled on the edge of the growth axis and is not in stratigraphical order with the other dating points. At the base of Qad-1, the growth rate is around 60 µm/a evolving to a higher rate around 150 µm/a and up to 500 µm/a in the upper part of the stalagmite. For the Qad-2 stalagmite, all the ages are in stratigraphical order and were used in the calculation of the age model. The growth rate at the base of Qad-2 is very high, reaching 650 µm/a and is reduced to 60 and 20 µm/a in the middle and upper part of the stalagmite.

6.2. Stable isotopic composition of calcite, modern water and fluid inclusions

Calcite $\delta^{18}O$ and $\delta^{13}C$ values were analysed at a multi-annual to decadal resolution. The $\delta^{18}O$ values for Qadisha record (Fig. 3) range from −5.7 ‰ to −7.5 ‰, with a mean of −6.8 ‰. The $\delta^{13}C$ values range from −6.2 ‰ to −8.6 ‰ around a mean of -7.5 ‰. Both $\delta^{18}O$ and $\delta^{13}C$ values generally co-vary during the entire period from ~9.1 to ~5.7 ka but are distinct in the medium and long-term trends. For example, the $\delta^{18}O$ values show an overall trend towards more positive values from early to the Mid-Holocene, unlike the $\delta^{13}C$ values that show a trend towards more negative values when reaching the Mid-Holocene. Significant variations are noticeable in the stable-isotope curves with clear $\delta^{18}O$ and $\delta^{13}C$ excursions around ~ 9.1, ~8.9, ~7.7, ~7.4-7.2, ~6.5 and ~5.9 ka.

Stable-isotopes of Qad-2 calcite dated at 0.005 ± 0.007 ka (calcite age between 1938 and 1952 CE) show an average $\delta^{13}C$ and $\delta^{18}O$ value of −7.2 ‰ and −6.6 ‰ respectively. On a comparative basis, present cave and spring water sampled in 2011 and 2014 in Qadisha Cave (Nehme et al., 2019) show average values of -8.6‰ for $\delta^{18}O_w$ and -46.9‰ for $\delta^{2}H_w$.

Table 2*. Qadisha fluid inclusions samples in chronological order (old to young). Stable-isotope measurements are shown in 1σ error. Measurements with an (*) are considered outliers due to a low water amount of less than 0.5* µl/g*. Apparent formation temperature was determined using the calcite-water fractionation factors after Kim and O'Neil. (1997).*

Qad_2 samples	Age of level [ka CE 1950]	Sample code	δH^2 [permil]	$\delta^{18}O$ [permil]	Volume [µl]	Mass [g]	Water amount [µl/g]	T_{fi} [°C]
Level B	~9.0-9.1	BQ_2_d	-41.70	-5.81	0.29	0.58	0.50	18.7±2.5
Level B	~9.0-9.1	BQ_2_b	-43.20	-7.65	0.73	0.78	0.94	10.3±2.5
Level B*	~9.0-9.1	BQ_2_a	-39.58	-5.53	0.23	0.72	0.32	20.1±2.5
Level A	~7.2-7.3	AQ_1	-42.82	-7.04	0.39	0.46	0.84	12.2±2.3
Level E*	~0.05	EQ_1	-19.46	-6.88	0.01	0.45	0.02	11.2±2.4

Average fluid inclusions $\delta^{18}O_w$ and δ^2H_w values of Qad-2 are -6.5 ‰ and -41.8 ‰, respectively. Samples taken at approximately the same level B in the stalagmite (~9.0-9.1 ka) show a certain variability of 3.6 ‰ for δ^2H and 2.6 ‰ for $\delta^{18}O$, between samples. The sample with the highest water yield shows the most negative $\delta^{18}O$ value. At ~7.2-7.3 ka, $\delta^{18}O_w$ is -7.0 ‰ and δ^2H_w is -42.8 ‰ (Table 2). Level E spanning a time period of the last century yielded a very low amount of water and was therefore rejected.

6.3. High resolution trace element data

Main trace element ratios presented in Fig. 3 are all above background levels. The overall sampling resolution is annual to multi-annual. The average elementary ratios show a slight shift between Qad-1 and Qad-2 with in general a higher variability for Qad-1. Mg/Ca ratios show a few significant shifts that are mirrored in most other investigated ratios (Fig. 3). Particularly strong trace elemental signals are visible around ~9.0-8.9 and ~7.7 ka, whereas weaker signals are noticeable at ~8.5, ~7.3 & ~7.1, ~6.6 and ~5.8 ka.

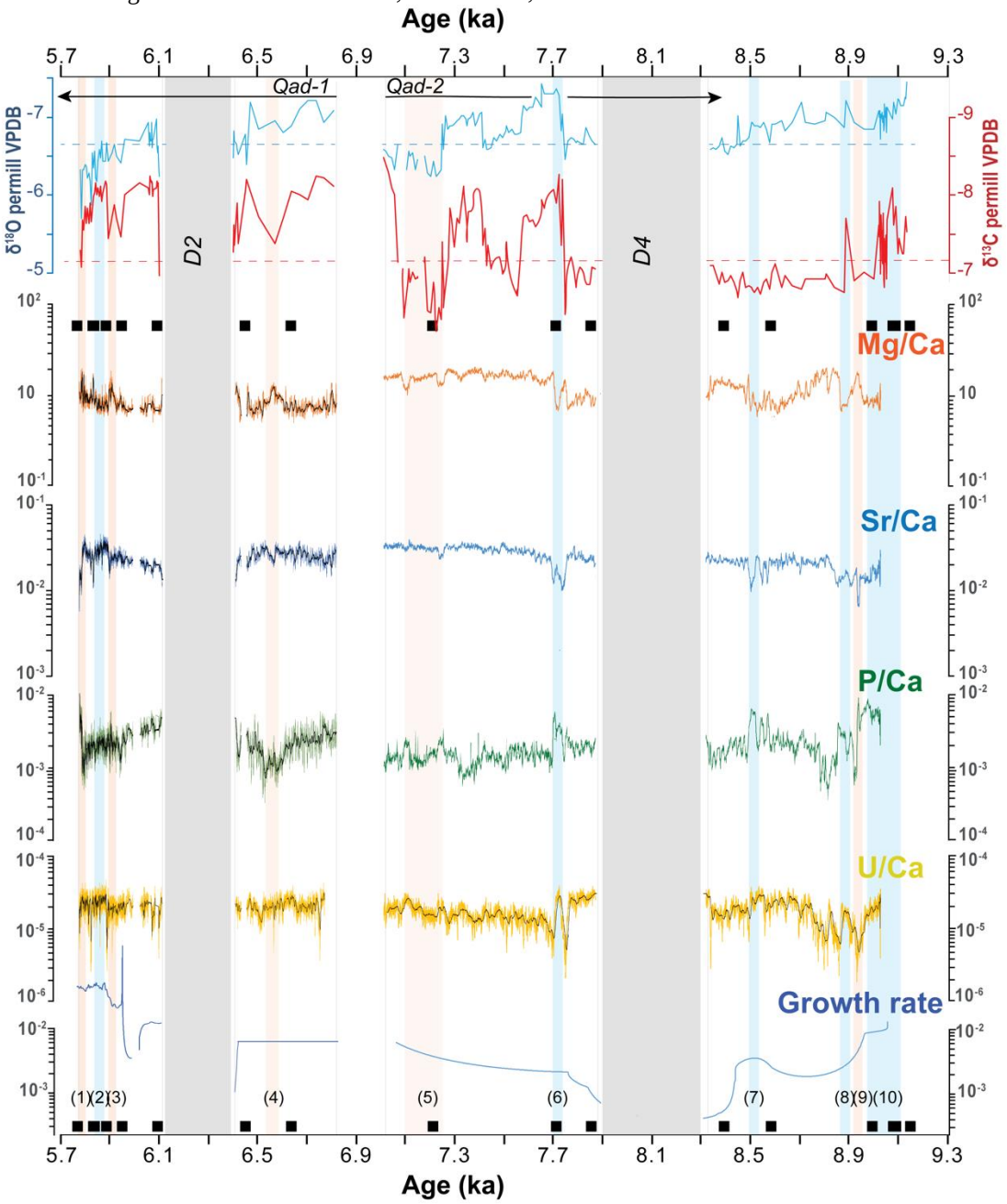

Figure 3: *$\delta^{18}O$ and $\delta^{13}C$ profiles of both Qad-1 and Qad-2 stalagmites with the trace elements curves (Mg/Ca, Sr/Sa, P/Ca, U/Ca) and a moving average curve (in black) for some of the trace elements. Growth rate is displayed in logarithmic scale. Both stable isotopes and trace elements data are plotted against time (yr CE 1950), modelled using StalAge. Black dots refer to the dating points and the grey shading to the identified discontinuities (D2, D4). Blue rectangles highlight significant variations towards wetter conditions in both stable isotopes and trace element data and orange rectangles highlight drier*

conditions. Dashed lines crossing $\delta^{18}O$ and $\delta^{13}C$ profiles indicate present-day values. Rapid dry and wet events are numbered from 1 to 10.

7. Discussion

7.1. Age growth behavior of the studied speleothems

Both stalagmites grew during the Holocene, roughly between 9.2 and 5.7 ka, one succeeding the other and suggesting favorable (humid and warm) conditions for stalagmite deposition at the high altitude of Qadisha cave. Although growth is relatively constant over most parts of the stalagmites, several hiatuses are observed. Former studies on stalagmites from Mt-Lebanon (Verheyden et al., 2008; Nehme et al., 2015; 2018) suggest that cave calcite precipitation and thus growth in the central Levant is conditioned by effective infiltration (Cheng et al., 2015). The growth stops may be site-specific but could also reflect unfavorable conditions for calcite deposition, such as dry conditions with low effective infiltration within the epikarst or scarser vegetation with less bio-vegetation activity. Based on the number of currently analyzed speleothems, one cannot make the distinction between one of the options.

Growth rates of both stalagmites are of the same order, reflecting similar drip rates and cave pCO_2. Similarities in the petrography of both speleothems corroborate consistent growth conditions. High growth rates of 0.15-0.6 mm/a between 5.8 and 6.1 ka and of 0.3-0.9 mm/a between 9.0 and 9.15 ka allow for annual and higher resolution climate reconstruction. Growth rates of 15-50 µm/a for most other parts of the record allows at least for multi-annual resolution using traditional micro-milling technique for stable isotope analysis. Two growth stops at 8.3-7.8 ka and 6.4-6.1 ka are supported by two clear petrographical discontinuities. The growth stops between 8.3 and 7.8 ka in Qad-2 stalagmite, although supported petrographically by a thin dust layer, is not supported by changes in other proxies prior or after the hiatus. If regional aridification characterized the 8.2 ka event, as inferred from the lowland Jeita Cave record (Cheng et al.,2015), then a combination of low infiltration and scarcer vegetation within the Qadisha karst basin would make speleothem growth highly unfavorable, plausibly leading to a centennial-scale hiatus. Such a hiatus is observable in Qad-2, but cannot be attributed confidently to climatic change.

Unlike the growth stop dated between 8.3 and 7.8 ka in Qad-2, the one dated between 6.5 and 6.1 ka in Qad-1 seems to be clearly framed by changes in stable-isotope values and trace elements. More positive $\delta^{18}O$ and $\delta^{13}C$ values suggest drier conditions prior and directly after the growth stop and may record unfavorable growth conditions, although prior calcite precipitation related to local factors at the drip rate may occur and other speleothems need to be studied to confirm our hypothesis. This seems also in agreement with a change towards increased Mg/Ca values, and decreased Sr/Ca values just prior and after the hiatus.

7.2. Interpreting the changes in geochemical proxies from Qadisha Cave

a- Speleothem $\delta^{18}O$ & $\delta^{13}C$

In the Levant, it is now widely established that the $\delta^{18}O$ signal is interpreted as related to effective recharge in the epikarst (precipitation amount vs evapotranspiration) and therefore infer to water balance (P-E) in the epikarst (Bar-Matthews et al., 2003; Verheyden et al., 2008; Cheng et al., 2015; Nehme et al., 2020). Higher infiltration (more positive P-E) is related to pronounced low-pressure systems with significant rainfall. Higher rainfall amounts are known to cause more negative rainfall $\delta^{18}O$ values (Bar-Matthews et al., 2003; Aouad et al., 2004) and reduced annual rainfall (with concomitant reduced P-E) to cause higher rainfall $\delta^{18}O$ values.

At mid-latitudes, $\delta^{13}C$ and growth rate in speleothems are related to biological CO_2 production, which is dependent on soil and vegetation conditions in the catchment (Genty et al., 2001a; 2001b). Warmer and wetter periods usually enhance the production of biogenic, $\delta^{13}C$-depleted CO_2 and increases the growth rate (Genty et al., 2001a; 2001b). Cold/dry conditions reduce the vegetation cover and the biogenic CO_2 supply. Lower/higher calcite $\delta^{13}C$ values and faster/slower growth rates are therefore usually indicative of soil development/disruptions and can be related to warmer-wetter/colder-drier conditions. An additional control on the $\delta^{13}C$ is exerted by the hydrological state of the aquifer. Partial dewatering of the drip-feeding system induces longer residence times and prior calcite precipitation, leading to higher $\delta^{13}C$ during drier periods (Fairchild and Baker, 2012).

The stable isotopic $\delta^{18}O$ values of both Qadisha stalagmites display a general trend from 8.5 to 5 ka towards more positive $\delta^{18}O$ values. This general $\delta^{18}O$ trend comprises three independent segments that include several rapid shifts towards negative values at ~9.1 ka (10), ~8.9 (8), ~8.5 (7) ~7.7 (6) ka and 5.8 (2) ka (Fig. 3). Such negative 'peaks' are interpreted as wet intervals with high effective recharge (high growth intervals of the stalagmites) and a positive water-balance (P-E) (Cheng et al., 2015). Rapid changes towards more positive $\delta^{18}O$ at ~9.0(9), ~7.1–7.2(5), ~6.6(4), ~5.9(3) and ~5.7(1) ka, are particularly well expressed and chronologically constrained. Some of these periods interpreted here as 'drying' events, particularly at ~9.0(9), are characterized unusually by high

growth rates. Such peculiar periods seem to indicate at least locally, a wet period as confirmed by negative (lower) $\delta^{13}C$ values, prior to the short dry period of ~80 years, but with still high growth rates. Albeit with low resolved growth rates compared to the resolution of geochemical proxies (annual for trace elements and decadal for the $\delta^{13}C$/ $\delta^{18}O$), such peculiar drying events preceded by short wet events reflect a rapid decadal variability, inferring to a shift in the distribution of effective infiltration.

b- Trace elements

In general, the (trace) element concentrations of Mg, Sr, P, and U in calcite are controlled by hydrological processes and less by cave temperature (Roberts et al., 1998). Speleothem Sr/Ca ratios constitute a sensitive proxy for infiltration changes in the epikarst, with higher values being recorded during times of reduced effective moisture availability (Fairchild and Treble, 2009). Other mechanisms can explain Sr mobility within the epikarst and include changes in weathering rates, aerosol input, soil activity that can induce high-frequency variability on short timescales (decadal to annual) (Verheyden et al., 2000; Fairchild et al., 2006; Sinclair et al., 2012; Baker et al., 2021). For Mg/Ca ratios in speleothems, it is common to attribute an increase as a response to prior calcite precipitation (PCP) during times periods of low effective infiltration (Verheyden et al., 2000; Tooth and Fairchild, 2003; McDermott et al., 2004; Fairchild et al., 2006). Since Sr/Ca ratios are similarly influenced by PCP, Mg and Sr ratios are often positively correlated.

An exception to this behavior is given in the presence of dolomitized limestone in the karst aquifer, which is the case in the Qadisha basin, where processes of incongruent calcite dissolution and/or differentiated soil input may play a role (Roberts et al., 1998; Hellstrom and McCulloch, 2000; Huang et al., 2001; Sinclair et al., 2012, Jamieson et al., 2016).

Phosphorous and U are less commonly studied but increasingly used as proxies in the speleothems archive. This element is generally mobilized from soils during early autumnal/winter storms. High P/Ca in speleothems reflect maximum soil infiltration during heavy rainfalls at the start of wet seasons (Borsato et al., 2007). The P/Ca ratio can be complemented by other palaeo-hydrological proxies such as Ba/Ca or U/Ca. U is generally leached from the bedrock during high rainfall events and results in high U/Ca into the calcite. (Ayalon et al., 1999; Treble, 2009)

In the Qadisha speleothems, the trace element concentrations vary at maximum by two orders of magnitude. Wet and dry episodes identified by stable-isotopes and growth rate changes (section 7.2.a, Fig. 3) can overall be linked to changes in the trace element concentration, with generally high Mg/Ca, and low Sr/Ca, P/Ca and U/Ca corresponding to higher stable-isotope values, suggesting an overall common driver, although with different sensitivities between proxies. Therefore, we assign in the Qadisha speleothems the periods with high $\delta^{13}C$/$\delta^{18}O$ and Mg (and generally low Sr, P and U) to dry periods, with a lower water recharge in the epikarst, and the opposite changes to wet periods. At 9.0 ka and 7.7 ka, significant changes in $\delta^{13}C$ and $\delta^{18}O$ values, as well as in U and P concentrations may suggest the occurrence of important flushing episodes.

7.3. Infiltration water isotopes based on fluid inclusion analysis

Isotope measurements of fluid inclusions water (δD; $\delta^{18}O_w$) can provide insights into the hydrological cycle and allow estimation of mineral formation temperatures. Three successful fluid inclusion analyses from Qad-2 stalagmite with water amount >0.5 µl/g were retained here (Table 2). $\delta^{18}O$ and δD values of water sampled in pools, cave streams and drip water inside Qadisha cave vary between -8.4 and -9.0, and between -45.7 ‰and -49.5 ‰, respectively. The d-excess of the cave water is between 21.4 and 22.6 ‰ (Nehme et al., 2019). As the cave water represents an average of the annual precipitation, rainfall values in contrast show a higher variability from -12.6 to +1.2 ‰ and -86 to +11.6 ‰ for $\delta^{18}O$ and δD values, respectively (Aouad et al., 2004). d-excess values are between 2 and 27 ‰ with an average close to that of the cave water (Aouad et al., 2004), indicating a generally higher d-excess for Lebanon compared to the GMWL. Although FI values fall within the modern-day range of rain water, compared to modern-day drip water from Qadisha, they show important variability. Especially, the samples from the B-level (9.0-9.1 ka) raise questions about the lateral coherency of the isotopic composition of FI water. The variability between different levels (B versus E) may be related to differences in isotopic composition of the rain and therefore the fluid inclusions. Overall, the results are more positive than today's isotopic composition of drip waters. Following our above interpretation, these values dated within the interval of 7.2-7.3 ka and 9.0-9.1 ka, represent isotopic values of water precipitated close to dry events (5) and (9) identified above based on their more positive calcite $\delta^{13}C$ and $\delta^{18}O$ values (Fig. 4) and may suggest short-term drier conditions in the generally wetter Early- to Mid-Holocene. A higher fraction of summer rainfall contribution to the water budget with a higher isotope value compared to winter snow with its lower isotopic composition (Aouad et al., 2004) may be another possibility to explain this isotopic observation. In Soreq Cave, Early-to Mid-Holocene fluid inclusion isotope values are comparable or slightly more negative compared to modern-day values

(Matthews et al., 2021). This contrasting effect could be related to Sapropel S1 that has a significant effect on the isotope values in the southern Levant (Bar-Matthews et al., 2003) but is not particularly expressed in the northern Levant (e.g. the Jeita record; Cheng et al., 2015) where rainfall amounts are generally higher. In addition, snowfall is of minor importance for the infiltration budget at Soreq cave whereas it is today the dominant water source in the region around Qadisha cave.

The fluid inclusion isotope values of various Early- to Mid-Holocene speleothems along the Levant become more negative from South (Soreq Cave) to the North (Qadisha Cave), in agreement with a dominating altitudinal effect and in addition by an increase in average rainfall towards the Lebanon mountains (Nehme et al., 2019). The difference in drip water $\delta^{18}O$ values between Soreq and Qadisha cave is ~4‰, which is close to the expected difference from altitude alone. The elevation difference is about 1400 m which explains an isotopic shift of 2.8-4.2 ‰ at a lapse rate of 0.2-0.3 ‰/100 m (Clark and Fritz, 1997). The difference between measured fluid inclusion isotope values of Holocene samples from the Soreq and Qadisha cave is similar. Although hardly resolvable with the current set of fluid inclusion data, rainfall amount could also play a role. For example, Mizpe Shelagim is situated almost at the same elevation as Qadisha cave, but about 120 km to the South and shows a more positive $\delta^{2}H$ value than Qad-2.

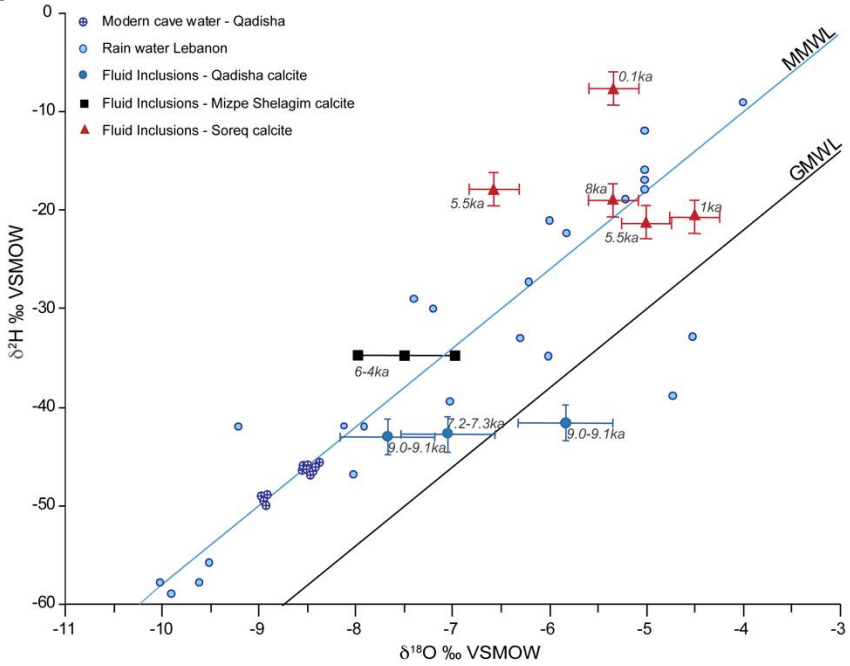

Figure 4. *Graph showing the fluid inclusion stable-isotope of Qadisha stalagmite (this study) in comparison with FI from Mizpe Shelagim (Ayalon et al., 2013) and Soreq record (Matthews et al., 2021), all plotted against the Global (Rozanski et al., 1993) and Mediterranean meteoric waterlines (Gat et al., 2003). Modern rain water of Lebanon (Aouad et al., 2005; Saad et al., 2005) are plotted in blue circles respectively. Modern cave water of Qadisha cave is plotted in crossed rectangles and circles respectively.*

7.4. The climatic conditions during the Holocene optimum

a- Global and regional drivers of climate variability during the Holocene Optimum

The Qadisha stalagmites grew from 9.2 to 5.7 ka, albeit with a discontinuous trend, and show a general tendency from more negative $\delta^{18}O$ values during the Early Holocene towards more positive $\delta^{18}O$ values at the end of the Holocene optimum. This trend reflects a change from a wetter (more positive P-E) towards a drier climate (reduced P-E) in this high-altitude area. This trend is also noticeable at low altitude, for example in the Jeita $\delta^{18}O$ record, and in other speleothem records from the Southern Levant, e.g., Mizpe Shelagim and Soreq Cave (Fig.5A). The carbon signal in Qadisha indicates values reaching -8‰ during wet peaks and shifts to -6‰ during dry events (Fig. 5B), reflecting a higher soil and vegetation activity during humid periods. The $\delta^{13}C$ curve overprints the short-term changes with a slow long-term increasing trend (Fig. 5B) towards more negative values when reaching the Mid-Holocene, suggesting overall improved bio-pedological soil activity in the Makmel mountains from 9 to 6 ka.

The two investigated Qadisha stalagmites started to grow during the period of maximum summer insolation (Berger and Loutre, 1991) and a high SST in the Eastern Mediterranean, reaching ~18°C during the Holocene optimum (Fig. 6) (Emeis et al., 2003; Scrivner et al., 2004). From 10 to 6.5 ka, the deposition of Sapropel 1 in the Eastern Mediterranean occurred as a result of increased discharge of the river Nile, leading to isotopically lighter

sea surface water. The contribution of the Mediterranean source effect as the only factor in the $\delta^{18}O$-depleted signals in terrestrial records has been debated in the last decades. Recent studies on Yammouneh lake (Develle et al., 2010), Soreq (Grant et al., 2016) and Zalmon caves (Keinan et al., 2019) show a contribution of rainfall amount in changes of the $\delta^{18}O$ signal throughout Glacial-Interglacial cycles and even during the sapropel events, by extracting the source signal (the $\delta^{18}O_{g.ruber}$) from the $\delta^{18}O_{calcite}$ of speleothems or $\delta^{18}O_{ostrac.}$ Signal of lake ostracods. An increased precipitation over Mt-Lebanon during the Sapropel event is noticeable with depleted $\delta^{18}O_{lake}$ (corrected from the source) signal reaching -11‰ in Yammouneh lake, from 9.2 to 8.3 ka. Likewise, the uncorrected $\delta^{18}O_{ostrac.}$ signal of the lowland Sagilik II peat record (Sekeryapan et al., 2020) in the northern part of the Levant, albeit a low-resolved curve, reach the most depleted ostracod $\delta^{18}O$ values between 9 and 7.7 ka. The well-dated lowland Jeita Cave record in central Lebanon show the most depleted values for the whole record around 8.5 ka, followed by a sharp $\delta^{18}O$ drop (less negative values) from 8.5 to 8 ka and then a general decrease with less negative $\delta^{18}O$ values until 5 ka.

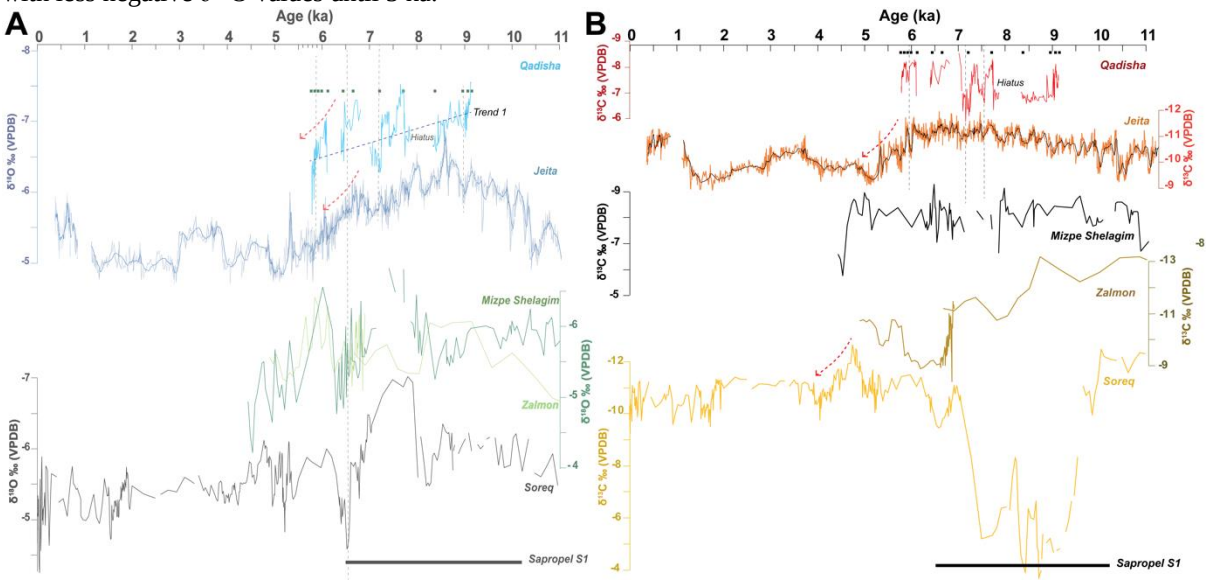

Figure 5. *Plots of the Qadisha stable-isotope curve in comparison with other speleothem records in the Levant. A. Carbon isotope curves. B. Oxygen isotope curves. Black dots represent U-Th dating points in the Qadisha record.*

More locally in the Makmel mountains, the Quercus pollen taxa in Al-Jurd peat core (Cheddadi and Khater, 2016), located 23 km North of Qadisha cave, show a relatively high pollen taxa from 10 to 8 ka, followed by a reduced Quercus pollen percentage from 8 to 6.5 ka, and marked later by an increase of Quercus pollen % at 6.5, 5.5, 4.5 and 3 ka (Fig. 6). Albeit a low-resolved curve, the pollen record of Al-Jurd peat core seems to show a higher percentage of Quercus pollen during the Mid-Holocene (6.5 to 3 ka) rather than in the Early-Holocene period from 9 to 6 as indicated by several speleothems. The Quercus Forest extension after 6.5 ka is rather puzzling in the local paleoclimate scheme of (speleothems) the Makmel mountains, but could suggest wetter/warmer conditions with improved bio-pedogenic activity in soils coeval with a reduced snow season and/or decreased snow cover enabling the extension of the forest. During the Early Holocene, slightly colder/dryer conditions (than the mid-Holocene) might have prevailed with the persistence of longer snow cover period, impacting the length of the plant growing season but enhancing speleothem growth with an important recharge from the snow melt during summer. Soil erosion is enhanced during short melt seasons on the long-term trend in the Makmel mountains, and would explain the reduced Quercus Forest in the area. In similar alpine context such as in Rio Martino cave, Piedmont Alps, Italy (Regiaterri et al., 2019), it was suggested that an increase in the persistence of snow cover may also impact the $\delta^{13}C$ by reducing the length of the plant growing season, leading to reduced biogenic CO_2 supply and therefore to less negative $\delta^{13}C$ signal in speleothems. Above the Qadisha site, the Cedar Forest stretching over same altitude than in El-Jurd site, may have had similar reduction/extension dynamics during the Early/Mid-Holocene and thus leading in general from $\delta^{13}C$ signal (avg: -7 ‰) in Qadisha speleothems in the Early-Holocene to a slightly more negative $\delta^{13}C$ signal (avg: -8 ‰) in the Mid-Holocene.

b- Centennial-scale climate variability

Rapid climatic changes of centennial scale are recorded in some of the highly-resolved stalagmites along the Levantine coast. Cheng et al., (2015) detected nine cold/dry events in the Jeita record during the Holocene coeval with those in the North Atlantic sediments (Bond et al., 2001). The Bond events in the Jeita record are interpreted as dry events inferred from both $\delta^{18}O$ and $\delta^{13}C$ variations (Cheng et al., 2015) (Fig. 5 and 6). Some of the events, such as the ~5.1 ka, noticeable in the Jeita record, is also recorded as a dry event in Anatolian Lake records (Roberts et al., 2011). The 8.2 ka, recorded in the Jeita stalagmite, corresponds to a $\delta^{18}O$ and $\delta^{13}C$ excursion (Fig.

4) in Soreq cave (Bar-Matthews et al., 2003). Such event is however not noticeable in other speleothem records along the Levantine coast, nor in Yammouneh lake (Develle et al., 2010). In Qadisha cave, the 8.2 ka cold event is not expressed or may be related to the growth stop.

Other events, at ~8.9-9.0 ka, ~7.1 and ~5.9 ka, (Fig. 4) in the Jeita record are also visible in the Qadisha record with more positive stable-isotope values (dry events), but with less clear changes in the related trace element pattern. In contrast, rapid climate changes interpreted as wet events in Qadisha Cave, such as the most prominent 7.7 ka wet period is not noticeable in the Jeita record but corresponds to the major peak in the Soreq record (Fig. 5A). The inconsistency in recording rapid climate change events between Levantine records may be due to different proxy resolution (e.g., smoothing in case of too low resolution) or differences in the local archive sensitivity on rapid climate changes.

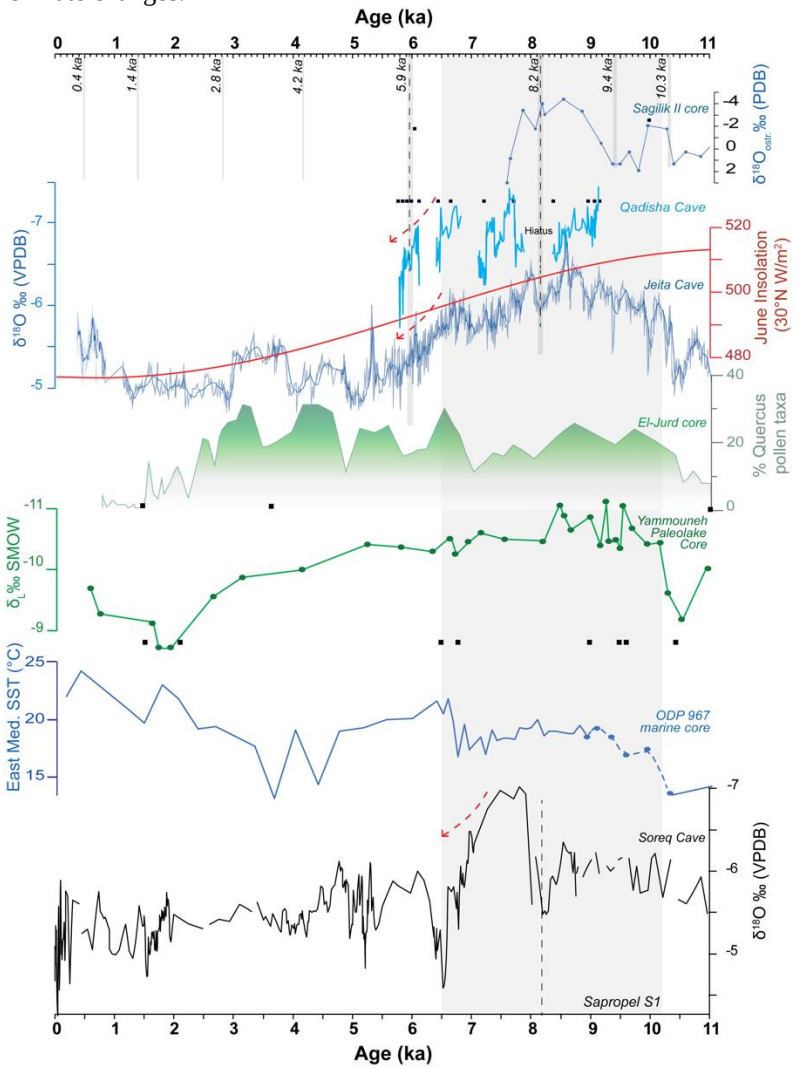

Figure 6. *Comparison of the Qadisha record with regional records in the EM region. From top to bottom: Sagilik II $\delta^{18}O_{ostracods}$, Turkey (Sekeryapan et al., 2020), Qadisha $\delta^{18}O_c$ record, Lebanon (this study) Jeita $\delta^{18}O_c$ record, Lebanon (Cheng et al., 2015), the Summer Insolation courve (Berger and Loutre, 1991), Quercus Pollen taxa % from El-Jurd Core (Cheddadi & Khater, 2016), $\delta^{18}O_L$ Yammouneh paleolake record (Develle et al. 2010), East Mediterranean SST, ODP 967 (Emeis et al., 2003; Scrivner et al., 2004), Soreq $\delta^{18}O_c$ record (Bar-Matthews et al., 2003)*

c- Altitudinal and snow cover effect on the significance of climate signals

In the Levant, most of the published speleothem records are located at low altitudes facing the Mediterranean Sea, except for Incesu and Mizpe Shelagim records located at 1615 m and 2180 m respectively. Only at Mizpe Shelagim a plausible link between the effect of snow cover at high altitudes and speleothem growth was established on Glacial-Interglacial timescales. During the Holocene interglacial, the snow cover in mountain areas participates actively in the epikarst water-budget, feed drip sites, and favor speleothem growth in caves located at high altitudes, as well as affect the vegetation dynamics. Whereas temperature remains close to 0°C during winter over large areas of Mt-Lebanon (Fayad and Gascoin, 2020), the soil beneath the snow does not freeze under

present winter conditions, except during exceptional cold events. Comparing the Qadisha records, with those located at low altitudes, helps in deciphering altitudinal trend and local particularities.

The Qadisha stalagmites show more negative $\delta^{18}O$ values (Fig. 5A) than those recorded by the Jeita stalagmite related to the altitudinal effect expressed in the rain and cave water isotopic signals (Nehme et al., 2019). Also, the contribution of the snow to the infiltration and the percolation water in caves (Aouad-Rizk et al., 2005) may lead to more negative drip water and calcite $\delta^{18}O$ values. Noteworthy is that the Qadisha stalagmites display a larger amplitude in the $\delta^{18}O$ changes and therefore have a more dynamic response to changes than the Jeita record. This behavior may be related to the higher altitude and the enhanced convective rainout at mountain ranges as well as to the generally lower $\delta^{18}O$ values of snow. An increase in low pressure systems can disproportionally increase the rainfall/snow amount at high-altitude mountain regions. Qadisha records can therefore indicate better, or at least more clearly rapid climate changes than the low-elevation Jeita speleothems. In contrast, short-term dry conditions may be better recorded by the lower-elevation archive sites as they are more sensitive to droughts and PCP which enhances the isotope and element signal. An example is the drought event recorded in Soreq, Mizpe Shelagim and Zalmon Cave around 6.5 ka which is well expressed in these caves, but less well expressed in Qadisha Cave.

More to the South, Zalmon and Soreq cave records indicate changes in the $\delta^{13}C$ values of more than 4‰ throughout the Holocene (Fig. 5B). This drastic shift in the $\delta^{13}C$ signal of Zalmon cave is mirrored by the $\delta^{13}C$ signals in other records, with a trend towards less negative $\delta^{13}C$ values by the end of the Holocene optimum. Although marked by a high $\delta^{13}C$ shift, the vegetation in northern Galilee indicates a reduced bio-pedological activity after 8.5 ka, whereas the soil activity seems to be less variable throughout the Holocene optimum in Jeita coastal site until 6 ka. In the case of Qadisha Cave, the carbon isotope signal reflects a higher sensitivity of the vegetation on humidity changes with step-changes (< 2‰), similar to Mizpe Shelagim (Mt Hermon). In Soreq cave located to the south, the shift to less negative carbon values that are closer to the bedrock signal throughout the Holocene optimum, is interpreted as reflecting a soil denudation by intensive storms. The vegetation cover appears to be more stable at Jeita and changes drastically only during larger climatic shifts (e.g. 6 ka), whereas the soil system at high-altitude sites (Qadisha and Mizpe Shelagim) is more sensitive to rapid changes in the water budget and the snow cover dynamics and indicate short-term erosional phases between 7 and 6 ka.

8-Conclusions

New stalagmites from Qadisha cave (Lebanon) located in the high Mt-Makmel, North of Mt-Lebanon, provide a well-dated record for the northern Levant with high-resolution geochemical proxies ($\delta^{18}O$ and $\delta^{13}C$ values, trace element concentrations). The Qadisha stalagmites grew from 9.2 to 5.7 ka, albeit with discontinuities, and show a general tendency from more negative $\delta^{18}O$ values during the Early Holocene towards more positive $\delta^{18}O$ values at the end of the Holocene optimum. This trend is in agreement with a change from a wetter to a drier climate in this high-altitude area. The $\delta^{13}C$ values show rapid shifts along the record and a decreasing trend towards more negative values when reaching the Mid-Holocene. The slight trend towards more negative values suggests overall improved bio-pedological soil activity in the Makmel mountains during the Mid-Holocene. Discrepencies between pollen data showing a wetter period at 7-6 ka than at 7-9 ka, unlike speleothems showing an overall wet Early Holocene are interpreted as related to a reduced snow cover season and thickness since 6.5 ka, explaining the extension of Quercus at 6.5 ka. On the short-term climate trend, Qadisha stalagmites record rapid dry and wet changes on centennial scale from 9 to 5 ka, with a tendency for drier conditions towards the mid-Holocene.

Qadisha record is in good agreement with other Levantine records, such as the one from Jeita Cave, showing overall more humid climate conditions from 9 to 7 ka in the region. After 7 ka, a drier climate seems to affect sites at both low and high-altitude areas. The Qadisha record reflects particularities of a mountainous climate compared to other records: *i)* more negative stable-isotopic values than the Jeita record due to the altitudinal rainout effect, *ii)* a larger amplitude in the oxygen isotopes reflecting a more dynamic response to rapid climate changes than records located at lower altitudes, *iii)* the effect of snow cover and duration, regulating the effective infiltration in the Makmel area.

9-Acknowledgments

This study and field mission was funded by the 2014 mobility fellowship program of the Belgian Federal Scientific Policy (BELSPO). We acknowledge the assistance of Saint-Joseph University of Beirut for facilitating the access to caves with the help of ALES (Association Libanaise d'Etudes Spéléologiques) and SCL (Spéléo-Club du Liban) and the support of both caving club members who collected water and calcite samples during field campaigns. Fluid inclusion measurements were supported by grant DFG KL2391/2-1 and Uranium-Thorium datings were funded by NSF Grant 2202913 to RLE.

10- CRediT author statement

C. Nehme: conceptualization, writing-original draft preparation, field investigation and sampling, analysis; **S. Verheyden**: conceptualization, field investigation, sampling, reviewing and editing; **T. Kluge**: analysis, software validation, funding, writing, review and editing; **F.H. Nader**: field investigation and sampling, review and editing ; **R.L. Edwards** : analysis, validation, funding; **H. Cheng** : analysis, funding ; **E. Eiche**: funding, supervision ; **Ph. Claeys**: funding, supervision.

11-References

Affolter S., Fleitmann D., Leuenberger M., 2014. New-on-line method for water isotope analysis of speleothem fluid inclusions using laser absorption spectroscopy (WS-CRDS). Clim. Past 10, 1291e1304.

Almogi-Labin A., Bar-Matthews M., Shriki D., Kolosovsky E., Paterne M., Schilman B., Ayalon A., Matthews A., 2009. Climatic variability during the last ~90 ka of the S. and N. Levantine Basin as evident from marine records and speleothems. Quat. Sci. Rev., 28(25-26), 2882-2896

Alpert P., Price C., Krichak S.O., Ziv B., Saaroni H., Osetinsky I., Kishcha P., 2005. Tropical teleconnections to the Mediterranean climate and weather. Adv. Geosci., 2, 157-160.

Aouad-Rizk A., Job J.O., Khalil S., Touma T., Bitar C., Bocquillon C., Najem W., 2005. $\delta^{18}O$ and $\delta^{2}H$ contents over Mt-Lebanon related to mass trajectories and local parameters. In: Isotopic composition of precipitation in the Mediterranean Basin in relation to air circulation patterns and climate. IAEA-TECDOC, 1453, 75-82.

Ayalon A., Bar-Matthews M., Sass E., 1998. Rainfall-recharge relationships within a karstic terrain in the Eastern Mediterranean semi-arid region, Israel: $\delta^{18}O$ and $\delta^{2}H$ characteristics. J. Hydrol. 207, 18-31.

Ayalon A., Bar-Matthews M., Kaufman A., 1999. Petrography, strontium, barium and uranium concentrations, and strontium and uranium isotope ratios in speleothems as palaeoclimatic proxies: Soreq Cave, Israel. Holocene 9, 715-722.

Ayalon A., Bar-Matthews M., Schilman B., 2004. Rainfall Isotopic Characteristics in Various Vites in Israel and the Relationships with the Unsaturated Zone Water. Israel Geological Survey. Report GSI/16/04.

Ayalon A., Bar-Matthews M., Frumkin A., Matthews A., 2013. Last Glacial warm events on Mt-Hermon: the southern extension of the Alpine karst range in the east Mediterranean, Quat. Sci. Rev., 59, 43–56.

Baker A., Mariethoz G., Comas- Bru L., Hartmann A., Frisia S., Borsato A., Asrat A., 2021. The Properties of Annually Laminated Stalagmites- A Global Synthesis. Rev. Geophy., 59(2), e2020RG000722.

Bar-Matthews M., Ayalon A., Matthews A., Sass E., Halicz L., 1996. Carbon and oxygen isotope study of the active water-carbonate system in a karstic Mediterranean cave: implications for paleoclimate research in semi-arid regions. Geochim. Cosmochim. Acta, 60, 337-347.

Bar-Matthews M., Ayalon A., Gilmour M., Matthews M., Hawkesworth C., 2003. Sea-land isotopic relationships from planktonic foraminifera and speleothems in the Eastern Mediterranean region and their implications for paleorainfall during interglacial interval, Geochim. Cosmochim. Acta, 67, 3181–3199.

Bar-Matthews M., Ayalon A., 2011. Mid-Holocene climate variations revealed by high-resolution speleothem records from Soreq Cave, Israel and their correlation with cultural changes. Holocene, 21(1), 163-171.

Bar-Matthews M., Keinan J., Ayalon A., 2019. Hydro-climate research of the late Quaternary of the Eastern Mediterranean-Levant region based on speleothems research–A review. Quat. Sci. Rev., 221, 105872.

Berger A., and Loutre M.F., 1991. Insolation values for the climate of the last 10 Millions years. Quat. Sci. Rev., 10, 297–317.

Bond G, Kromer B, Beer J. et al., 2001. Persistent solar influence on North Atlantic climate during the Holocene. Science, 294, 2130–2136.

Borsato A., Frisia S., Fairchild I.J., Somogyi A., Susini J., 2007. Trace element distribution in annual stalagmite laminae mapped by micrometer-resolution X-ray fluorescence: implications for incorporation of environmentally significant species. Geochim. Cosmochim. Acta, 71(6), 1494-1512.

Brayshaw D.J., Rambeau C.M., Smith S.J., 2011. Changes in Mediterranean climate during the Holocene: Insights from global and regional climate modelling. Holocene, 21(1), 15-31.

Burstyn Y., Martrat B., Lopez J.F., Iriarte E., Jacobson M.J., Lone M.A., Deininger M., 2019. Speleothems from the Middle East: an example of water limited environments in the SISAL database. Quaternary 2, 2, 16.

Burstyn Y., Shaar R., Keinan J., Ebert Y., Ayalon A., Bar-Matthews M., Feinberg J.M., 2022. Holocene wet episodes recorded by magnetic minerals in stalagmites from Soreq Cave, Israel. Geology 50, 3, 284-288.

Carolin S.A., Walker R.T., Day C.C., Ersek V., Sloan R.A., Dee M.W., Talebian M., Henderson G.M., 2019. Precise timing of abrupt increase in dust activity in the EM coincident with 4.2ka social change. Proc. Natl. Acad. Sci. USA 116, 67–72.

Cheng H., Zhang P.Z., Spötl C., Edwards R.L., Cai Y.J., Zhang D.Z., Sang W.C., Tan M., An Z.S., 2012, The climatic cyclicity in semiarid-arid central Asia over the past 500,000 years. Geophys. Res. Lett., 39, L01705.

Cheng H., Edwards R.L., Shen C.C., Polyak V.J., Asmerom Y., Woodhead J., Hellstrom J., Wang Y., Kong X., Spötl C., Wang X., 2013. Improvements in 230 Th dating, 230 Th and 234 U half-life values, and U–Th isotopic measurements by multi-collector inductively coupled plasma mass spectrometry. Earth Planet Sci. Lett., 371, 82-91.

Cheng H., Sinhac A., Verheyden S., Nader F.H., Li X.L., Zhang P.Z., Yin J.J., Yi L., Peng Y.B., Rao Z.G., Ning Y.F., Edwards R.L., 2015. The climate variability in northern Levant over the past 20,000 years. Geophys. Res. Lett., 42, 8641-8650.

Cheddadi R., Khater C., 2016. Climate change since the last glacial period in Lebanon and the persistence of Mediterranean species. Quat. Sci. Rev., 150, 146-157.

Dansgaard, W., 1964. Stable isotopes in precipitation, Tellus, 16, 436– 468.

Demeny A., Kele S., Siklosy Z., 2010. Empirical equations for the temperature dependence of calcite- water oxygen isotope fractionation from 10 to 70° C. Rapid Commun. Mass Spectrom, 24(24), 3521-3526.

Daëron M., Drysdale R.N., Peral M., Huyghe D., Blamart D., Coplen T.B., Zanchetta G., 2019. Most Earth-surface calcites precipitate out of isotopic equilibrium. Nature Commun., 10(1), 1-7.
Develle A.L., Herreros J., Vidal L., Sursock A. Gasse F., 2010. Controlling factors on a paleo-lake oxygen isotope record (Yammoûneh, Lebanon) since the Last Glacial Maximum. Quat. Sci. Rev., 29(7), 865-886.
Dubertret L., 1975. Introduction à la carte géologique au 50.000e du Liban. Notes et Mémoires sur le Moyen-Orient, 23, 345–403.
Edgell H.S., 1997. Karst and hydrogeology of Lebanon. Carbonates Evaporites, 12 (2), 220-235.
Edwards R.L., Chen J.H., Ku T.L., Wasserburg G.J., 1987. Precise timing of the last interglacial period from mass spectrometric determination of ^{230}Th in corals. Science, 236, 1547–1553.
Emeis K.C., Schulz H., Struck U., Rossignol-Strick M., Erlenkeuser H., Howell M.W., Kroon D., Mackensen A., Ishizuka S., Oba T., Sakamoto T., Koizumi I., 2003. Eastern Mediterranean surface water temperatures and ^{18}O during deposition of sapropels in the late Quaternary. Paleoceanogr., 18, 1005–1029.
Erkan G., Bayari C.S., Fleitmann D., Cheng H., Edwards L., Özbakir M., 2022. Late Pleistocene–Holocene climatic implications of high- resolution stable isotope profiles of a speleothem from S. Central Anatolia, Turkey. J. Quat. Sci. 37, 3, 503-515.
Fairchild I.J., Borsato A., Tooth A.F., Frisia S., Hawkesworth C.J., Huang Y., Spiro B., 2000. Controls on trace element compositions of carbonate cave waters: implications for speleothem climatic records. Chem. Geol., 166(3-4), 255-269.
Fairchild I.J., Smith C.L., Baker A., Fuller L., Spötl C., Mattey D., McDermott F., 2006. Modification and preservation of environmental signals in speleothems, Earth Sci. Rev., 75, 105–153.
Fairchild I.J., Treble P.C., 2009. Trace elements in speleothems as recorders of environmental change. Quat. Sci. Rev., 28(5-6), 449-468.
Fairchild I.J. and Baker A., 2012. Speleothem science-From processes to past environments. Quat. Geosci. Series, Wiley-Blackwell, 3–370
Fayad A., Gascoin S., 2020. The role of liquid water percolation representation in estimating snow water equivalent in a Mediterranean mountain region (Mt-Lebanon). Hydrol. Earth Syst. Sci., 24(3), 1527-1542.
Finné M., Holmgren K., Sundqvist H.S., Weiberg E., Lindblom M., 2011. Climate in the eastern Mediterranean, and adjacent regions, during the past 6000 years–A review. J. Archaeol. Sci., 38(12), 3153-3173.
Flohr P., Fleitmann D., Zorita E., Sadekov A., Cheng H., Bosomworth M., Edwards R.L., Matthews W., Matthews R, 2017. Late Holocene droughts in the Fertile Crescent recorded in a speleothem from N. Iraq. Geophys. Res. Lett. 44, 1528–1536.
Frumkin A., Ford D.C., Schwarcz H., 2000. Paleoclimate and vegetation of the Last Glacial cycles in Jerusalem from a speleothem record. Global Biogeochem. Cycles 14, 863–870.
Frumkin A., Stein M., Goldstein S.L., 2022. High resolution environmental conditions of the last interglacial (MIS5e) in the Levant from Sr, C and O isotopes from a Jerusalem stalagmite. Palaeogeogr. Palaeoecol. Paleoclim., 586, 110761.
Gasse F., Vidal L., Van Campo E., Demory F., Develle A.-L., Tachikawa K., Elias A., Bard E., Garcia M., Sonzogni. C., Thouveny N., 2015. Hydroclimatic changes in northern Levant over the past 400.000 years, Quat. Sci. Rev., 111, 1–8.
Gat J.R., Klein B., Kushnir Y., Roether W., Wernli H., Yam R., Shemesh A., 2003. Isotope composition of air moisture over the Mediterranean Sea: an index of the air–sea interaction pattern. Tellus, Series B-Chemical & Physical Meteorology, 55 (5), 953-965.
Genty D., Baker A., Massault M., Proctor C., Gilmour M., Pons-Branchu E., Hamelin B., 2001a. Dead carbon in stalagmites: carbonate bedrock paleodissolution vs ageing of soil organic matter. Implications for ^{13}C variations in speleothems. Geochim. Cosmochim. Acta, 65(20), 3443-3457.
Genty D., Baker A., Vokal B., 2001b. Intra- and inter-annual growth rate of modern stalagmites. Chem. Geol. 176(1–4), 191–212.
Genty D., Blamart D., Ouahdi R. Gilmour M., 2003. Precise dating of Dansgaard-Oeschger climate oscillations in western Europe from stalagmite data. Nature, 421(6925).
Göktürk O.M., Fleitmann D, Badertscher S et al., 2011. Climate on the southern Black Sea coast during the Holocene: implications from the Sofular Cave record. Quat. Sci. Rev., 30, 2433–2445.
Grant K.M., Rohling E.J., Bar-Matthews M., Ayalon A., Medina-Elizalde M., Bronk Ramsey C., Satow C., Roberts A.P., 2012. Rapid coupling between ice volume and polar temperature over the past 150 ka, Nature, 491, 744–747.
Grant K.M., Grimm R., Mikolajewicz U., Marino G., Ziegler M., Rohling E.J., 2016. The timing of Mediterranean sapropel deposition relative to insolation, sea- level and African monsoon changes. Quat. Sci. Rev., 140, 125e141.
Hajjar L., Haïdar-Boustani M., Khater C., Cheddadi R., 2010. Environmental changes in Lebanon during the Holocene: Man vs. climate impacts. J. Arid Env., 74(7), 746-755.
Hellstrom J.C., McCulloch M.T., 2000. Multi-proxy constraints on the climatic significance of trace element records from a New Zealand speleothem. Earth Planet Sci. Lett., 179(2), 287-297.
Huang H.M., Fairchild I.J., Borsato A., Frisia S., Cassidy N.J., McDermott F., Hawkesworth C.J., 2001. Seasonal variations in Sr, Mg and P in modern speleothems (Grotta di Ernesto, Italy). Chem. Geol. 175, 429–448.
Jacobson M.J., Flohr P., Gascoigne A., Leng M.J., Sadekov A., Cheng H., Fleitmann D., 2021. Heterogenous late Holocene climate in the Eastern Mediterranean—The Kocain Cave record from SW Turkey. Geophys. Res. Lett., 48(20).
Jamieson R.A., Baldini J.U., Brett M.J., Taylor J., Ridley H.E., Ottley C.J., Prufer K.M., Jasper A.Wassenburg J.A., Scholz D., Breitenbach S.F. (2016). Intra-and inter-annual uranium concentration variability in a Belizean stalagmite controlled by prior aragonite precipitation: A new tool for reconstructing hydro-climate using aragonitic speleothems. Geochim. Cosmochim. Acta, 190, 332-346.
Jochum K.P., Scholz D., Stoll B., Weis U., Wilson S.A., Yang Q., Andreae M.O., 2012. Accurate trace element analysis of speleothems and biogenic calcium carbonates by LA-ICP-MS. Chem. Geol., 318, 31-44.
Jochum K.P., Pfänder J., Woodhead J.D., Willbold M., Stoll B., Herwig K., Hofmann A.W., 2005. MPI- DING glasses: New geological reference materials for in situ Pb isotope analysis. Geochem., Geophys., Geosyst., 6(10)

Jones M.D., Roberts C.N., 2008. Interpreting lake isotope records of Holocene environmental change in the Eastern Mediterranean. Quat. Int., 181, 32–38.

Kallel N., Duplessy J.-C., Labeyrie L., Fontugne M., Paterne M., Montacer M., 2000. Mediterranean pluvial periods and sapropel formation during the last 200.000 years, Palaeogeogr. Palaeoecol. Paleoclim., 157, 45–58.

Kaniewski D., Marriner N., Cheddadi R., Fischer P.M., Otto T., Luce F., Van Campo E., 2020. Climate change and social unrest: A 6,000- year chronicle from the eastern Mediterranean. Geophys. Res. Lett., 47(7), e2020GL087496.

Keinan J., Bar-Matthews M., Ayalon A., Zilberman T., Agnon A., Frumkin A., 2019. Paleoclimatology of the Levant from Zalmon Cave speleothems, the northern Jordan Valley, Israel. Quat. Sci. Rev 220, 142-153.

Kim S.T. and O'Neil J.R., 1997. Equilibrium and nonequilibrium oxygen isotope effects in synthetic carbonates. Geochim. Cosmochim. Acta, 61(16): 3461-3475.

Kiro Y., Goldstein S.L., Kushnir Y., Olson J.M., Bolge L., Lazar B., Stein M., 2020. Droughts, flooding events, and shifts in water sources and seasonality characterize last interglacial Levant climate. Quat. Sci. Rev., 248, 106546.

Koeniger P., Margane A., Abi-Rizk J., Himmelsbach T., 2017. Stable isotope based mean catchment altitudes of springs in the Lebanon Mountains. Hydrol. Proc., 21, 3708-3718.

Masson-Delmotte V., Schulz M., Abe-Ouchi A., Beer J., Ganopolski A., Gonzalez Rouco J.F., Jansen E., Lambeck K., Luterbacher J., Naish T., Osborn T., Otto-Bliesner B., Quinn T., Ramesh R., Rojas M., Shao X., Timmermann A., 2013. Information from Paleoclimate Archives, In: Climate change 2013: the physical science basis: Contribution of Working Group I to the Fifth Assessment Report of the Intergovernmental Panel on Climate Change. Cambridge University Press, 383-464.

McDermott F., 2004. Palaeoclimate reconstruction from stable isotope variations in speleothems: a review. Quat. Sci. Rev., 23(7-8), 901-918.

Mischel S.A., Scholz D., Spötl C., Jochum K.P., Schröder-Ritzrau A., Fiedler S., 2017. Holocene climate variability in Central Germany and a potential link to the polar North Atlantic: a replicated record from three coeval speleothems. Holocene, 27(4), 509-525

Migowski C., Stein M., Prasad S., Negendank J.F.W., Agno, A., 2006. Holocene climate variability and cultural evolution in the Near East from the Dead Sea sedimentary record. Quat. Res. 66 (3), 421–431.

Musgrove M., Banner J.L., 2004. Controls on the spatial and temporal variability of vadose dripwater geochemistry: Edwards Aquifer, central Texas. Geochim. Cosmochim. Acta, 68(5), 1007-1020.

Nader F.H., Abdel-Rahman A.F.M., Haidar A.T., 2006. Petrographic and chemical traits of Cenomanian platform carbonates (central Lebanon): implications for depositional environments. Cretac. Res., 27(5), 689-706.

Nehme C., Verheyden S., Noble S.R., Farrant A.R., Sahy D., Hellstrom J., Delannoy J.J. Claeys P., 2015. Reconstruction of MIS 5 climate in the central Levant using a stalagmite from Kanaan Cave, Lebanon. Clim. Past, 11, 1785-1799.

Nehme C., Verheyden S., Breitenbach S.F., Gillikin D.P., Verheyden A., Cheng H., Noble S., Farrant A., Sahy D., Salem Gh, Ph Clayes, 2018. Climate dynamics during the penultimate glacial period recorded in a speleothem from Kanaan Cave, Lebanon (central Levant). Quat. Res. 90 (1), 10-25.

Nehme C., Verheyden S., Nader F.H., Adjizian-Gerard J., Genty D., De Bont K., Clayes P., 2019. Cave dripwater isotopic signals related to the altitudinal gradient of Mt-Lebanon: implication for speleothem studies. Int. J. Speleol. 48 (1), 1-8.

Orland I.J., BurstynY., Bar-Matthews M., Kozdon R., Ayalon A., Matthews A., Valley J.W., 2014. Seasonal climate signals (1990–2008) in a modern Soreq Cave stalagmite as revealed by high-resolution geochemical analysis. *Chemical Geol.*, *363*, 322-333.

Roberts M.S., Smart P.L., Baker A., 1998. Annual trace element variations in a Holocene speleothem. Earth Planet Sci. Lett., 154(1-4), 237-246.

Robinson S.A., Black S., Sellwood B.W., & Valdes P.J., 2006. A review of palaeoclimates and palaeoenvironments in the Levant & East. Mediterranean from 25 to 5 ka BP: setting the environmental background for the evolution of human civilisation. Quat. Sci. Rev., 25(13-14), 1517-1541.

Rohling E.J., Cane T.R., Cooke S., Sprovieri M., Bouloubassi I., Emeis K.C., Schiebel R., Kroon D., Jorissen F.J., Lorre A., Kemp A.E.S., 2002. African monsoon variability during the previous interglacial maximum. Earth Planet Sci. Lett., 202, 61-75.

Rossignol-Strick M., Paterne M., 1999. A synthetic pollen record of the eastern Mediterranean sapropels of the last 1 Ma: implications for the time-scale and formation of sapropels. Marine Geol., 153(1–4), 221–237.

Rowe PJ, Mason JE, Andrews JE et al. 2012. Speleothem isotopic evidence of winter rainfall variability in northeast Turkey between 77 and 6 ka. Quat. Sci. Rev., 45, 60–72.

Rowe P.J., Wickens L.B., Sahy D., Marca A.D., Peckover E., Noble S., Ozkul M., Baykara M.O., Millar I.L., Andrews J.E., 2020. Multi-proxy speleothem record of climate instability during the early last interglacial in southern Turkey. Palaeogeogr. Palaeoclimatol. Palaeoecol. 538, 109422.

Roberts N, Eastwood WJ, Kuzucuoğlu C et al. 2011. Climatic, vegetation and cultural change in the Eastern Mediterranean during the mid- Holocene environmental transition. Holocene, 21, 147–162.

Roberts N., Moreno A., Valero-Garcés B.L., Corella J.P., Jones M., Allcock S., Türkeş M., 2012. Palaeolimnological evidence for an east–west climate see-saw in the Mediterranean since AD 900. Glob. Planet. Change, 84, 23-34.

Rozanski, K., Araguas, L., and Gonfiantini, R., 1993. Isotopic patterns in modern global precipitation, in: Climate Change in Continental Isotopic Record, Geophysical Monograph Series, Washington DC, AGU, 78, 1–37.

Saad Z., V. Kazpard A.G. Samrani El., Slim K., 2005. Chemical and isotopic composition of rainwater in coastal and highland regions in Lebanon. J. Env. Hydrol., 13, 1-11.

Scrivner A.E., Vance D., Rohling E.J., 2004. New neodymium isotope data quantify Nile involvement in Mediterranean anoxic episodes. Geology 32, 565-568, 2004.

Scholz D., Hoffmann D.L., 2011. StalAge–An algorithm designed for construction of speleothem age models. Quat. Geochron., 6(3-4), 369-382.

Şekeryapan C., Streuman H.J., van der Plicht J., Woldring H., van der Veen Y., Boomer I., 2020. Late Glacial to mid-Holocene lacustrine ostracods from S. Anatolia, Turkey: a palaeoenvironmental study with pollen & stable isotopes. Catena 188, 5-11.

Shabaan A., Houhou R., 2015. Drought or humidity oscillations? The case of coastal zone of Lebanon. J. Hydrol., 529, 1768-1775

Sinclair D.J., Banner J.L., Taylor F.W., Partin J., Jenson J., Mylroie J., Miklavič B., 2012. Magnesium and strontium systematics in tropical speleothems from the Western Pacific. Chem. Geol., 294, 1-17.

Sinha A., Kathayat G., Weiss H., Li H., Cheng H., Reuter J., Edwards R.L., 2019. Role of climate in the rise and fall of the Neo-Assyrian Empire. Sci. Adv. 5, 11, 6656

Telesca L., Shaban A., Gascoin S., Darwich T., Drapeau L., El Hage M., Faour G., 2014. Characterization of the time dynamics of monthly satellite snow cover data on Mountain Chains in Lebanon. J. Hydrol., 519, 3214-3222

Torfstein A., Goldstein S.L., Stein M., Enzel Y., 2013a. Impacts of abrupt climate changes in the Levant from Last Glacial Dead Sea levels. Quat. Sci. Rev., 69, 1-7.

Torfstein A., Goldstein S.L., Kagan E.J., Stein M., 2013b. Integrated multi-site U–Th chronology of the last glacial Lake Lisan. Geochim. Cosmochim. Acta, 104, 210-231.

Tooth A.F., Fairchild I.J., 2003. Soil and karst aquifer hydrological controls on the geochemical evolution of speleothem-forming drip waters, Crag Cave, southwest Ireland. J. Hydrol., 273(1-4), 51-68.

Treble P., Shelley J.M.G., Chappell J., 2003. Comparison of high resolution sub-annual records of trace elements in a modern (1911–1992) speleothem with instrumental climate data from SW Australia. Earth Planet Sci. Lett., 216(1-2), 141-153.

Tremaine D.M., Froelich P.N., Wang Y., 2011. Speleothem calcite farmed in situ: Modern calibration of $\delta^{18}O$ & $\delta^{13}C$ paleoclimate proxies in a continuously monitored natural cave system. Geochim. Cosmochim. Acta, 75, 4929-4950.

Ulbrich U., Lionello P., Belusic D., Jacobeit J., Knippertz P., Kuglitsch F.G., Leckebusch G.C., Luterbacher J., Maugeri M., Maheras P., et al. 2012. Climate of the Mediterranean: Synoptic Patterns, Temperature, Precipitation, Winds, and Their Extremes. In Lionello, P. (Ed.), The Climate of the Mediterranean Region: From the Past to the Future, Elsevier, Amsterdam, 301–346.

Ünal-İmer E., Shulmeister J., Zhao J.X., Uysal I.T., Feng Y.X., Nguyen A.D., Yüce G., 2015. An 80 ka long continuous speleothem record from Dim Cave, SW Turkey with paleoclimatic implications for the East. Mediterranean. Sci. Rep., 5, 13560.

Van Zeist W., Woldring H., 1980. Holocene vegetation and climate of northwestern Syria. Palaeohistoria, 111-125.

Verheyden S., Keppens E., Fairchild I.J., McDermott F., Weis D., 2000. Mg, Sr and Sr isotope geochemistry of a Belgian Holocene speleothem: implications for paleoclimate reconstructions. Chem. Geol., 169(1-2), 131-144.

Verheyden S., Nader F.H., Cheng H.J., Edwards L.R., Swennen R., 2008. Paleoclimate reconstruction in the Levant region from the geochemistry of a Holocene stalagmite from the Jeita cave, Lebanon. Quat. Res., 70, 368–381

Weißbach T., 2020. Spectroscopic Isotope Ratio Analysis on Speleothem Fluid In- clusions - Analytics and Paleoclimatic Case Studies. PhD thesis. Heidelberg University, p. 225. https://doi.org/10.11588/heidok.00028559

Xoplaki E., González-Rouco J.F., Luterbacher J., Wanner H., 2004. Wet season Mediterranean precipitation variability: influence of large-scale dynamics and trends. Clim. Dyn., 23(1), 63-78.

Yasuda Y., Kitagawa H., Nakagawa T., 2000. The earliest record of major anthropogenic deforestation in the Ghab Valley, northwest Syria: a palynological study. Quat. Int., 73, 127-136.

Ziv B., Saaroni H., Romem M., Heifetz E., Harnik N., Baharad. A., 2010. Analysis of conveyor belts in winter Mediterranean cyclones. Theoretical Appl. Clim., 99, 441-455.

Editor’s comments

1. Please include (i.e., repeat) the abstract in the text of the manuscript itself.
this was done in the revised final draft

2. I believe "northern Lebanon" (as in the title), not "Northern Lebanon" is correct--unless the latter is a formally defined locality. Please maintain consistency throughout the manuscript.
the term Northern was corrected in the text and the capitalized word was replaced by “northern”

3. The journal doesn't use "kyr", just "ka" (thus, for example, the "8.2 ka event")
Kyr was replaced by ka in the text.

4. Do you really need two dozen citations on lines 59-63? Unless this is a review article, your point could surely be made with a more selective list.
the list was shortened and the unnecessary citations were removed from the reference list

5. If you use "CE" then "yr" is extraneous. See, for example, line 269. Although the journal doesn't have formal guidance, "CE 1950" is a more intuitive rendering than "1950 CE". In any case, maintain consistency throughout.
In the text, the ages were converted all to ka and the term “kyr” was replaced by “ka”. See correction model in lines 283, 285 and 302.

6. Figure 1a needs lat/long tics.
This was added in figure 1

7. Tables 1 and 2 need corrected headings for the ages.
The corrected reference to AGE was changed in the headings of table 1 and 2.

8. Figures 2, 3, 5, and 6 have four different ways of expressing what may (or may not) be the same thing. If you're giving an AGE, then simply "yr" (or "ka"), or if identifying the datum is critical, "yr (before CE 1950)". If you're giving a DATE, then "Date (CE)" would be correct. You should probably choose one framework and stick with it for all figures. In any case, no "yrs" and no "kyr".
In the figures, the reference to ages in the axis was changed into “Age (ka)”. only in figure 2, we put Age (ka before CE 1950) and the figure 2 refers to the age model.

Figure 1

Click here to access/download;Figure;Fig.1_Location.png

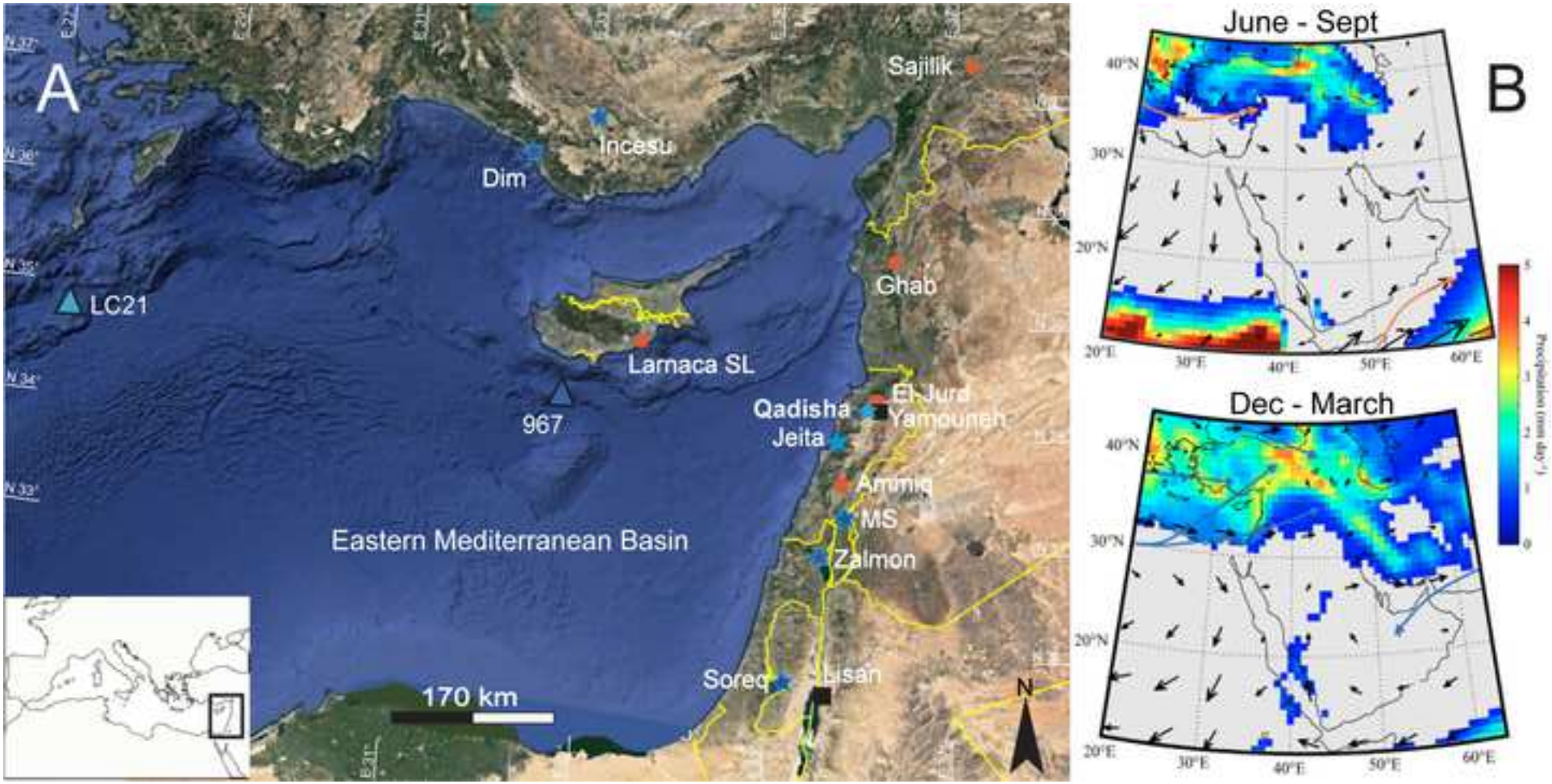

Figure 2

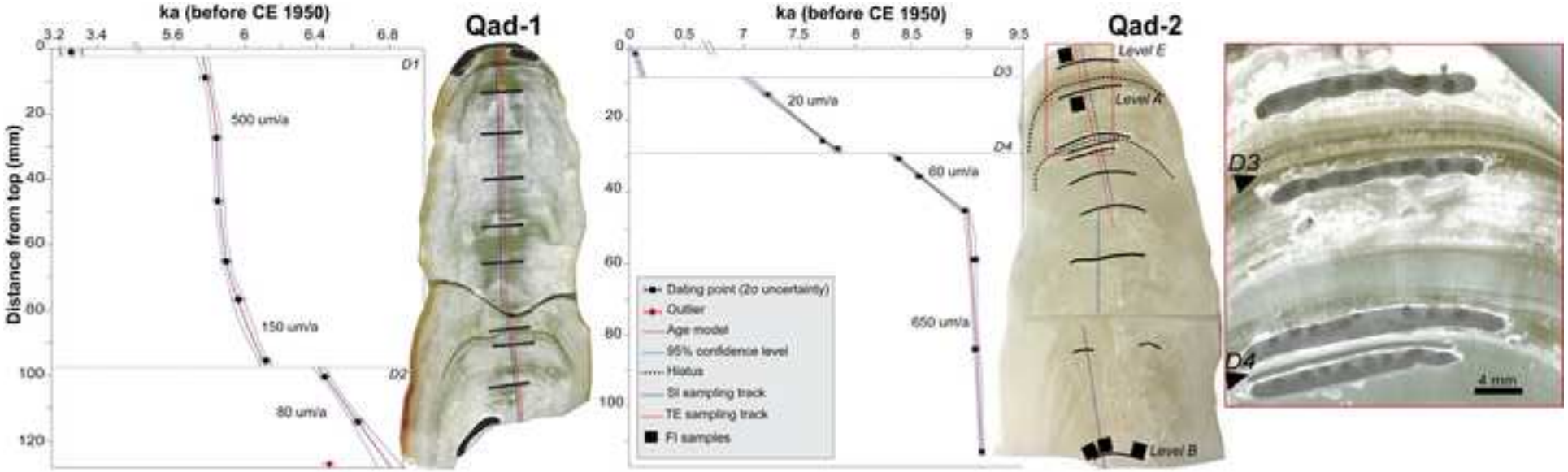

Figure 3

Click here to access/download;Figure;Fig.3_Dataset_Qad_All_final.png

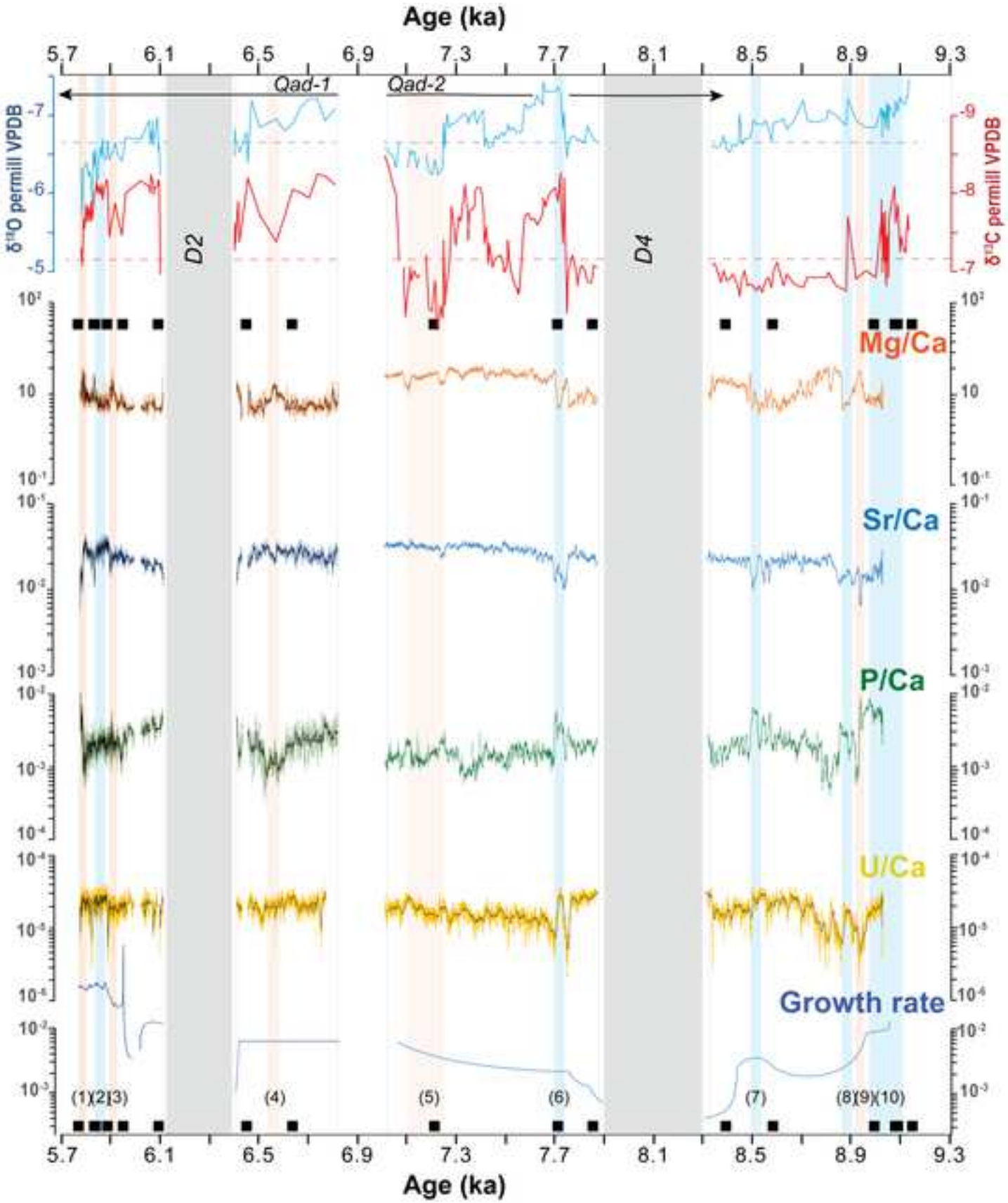

Figure 4

Click here to access/download;Figure;Fig.4_FI_regional.png

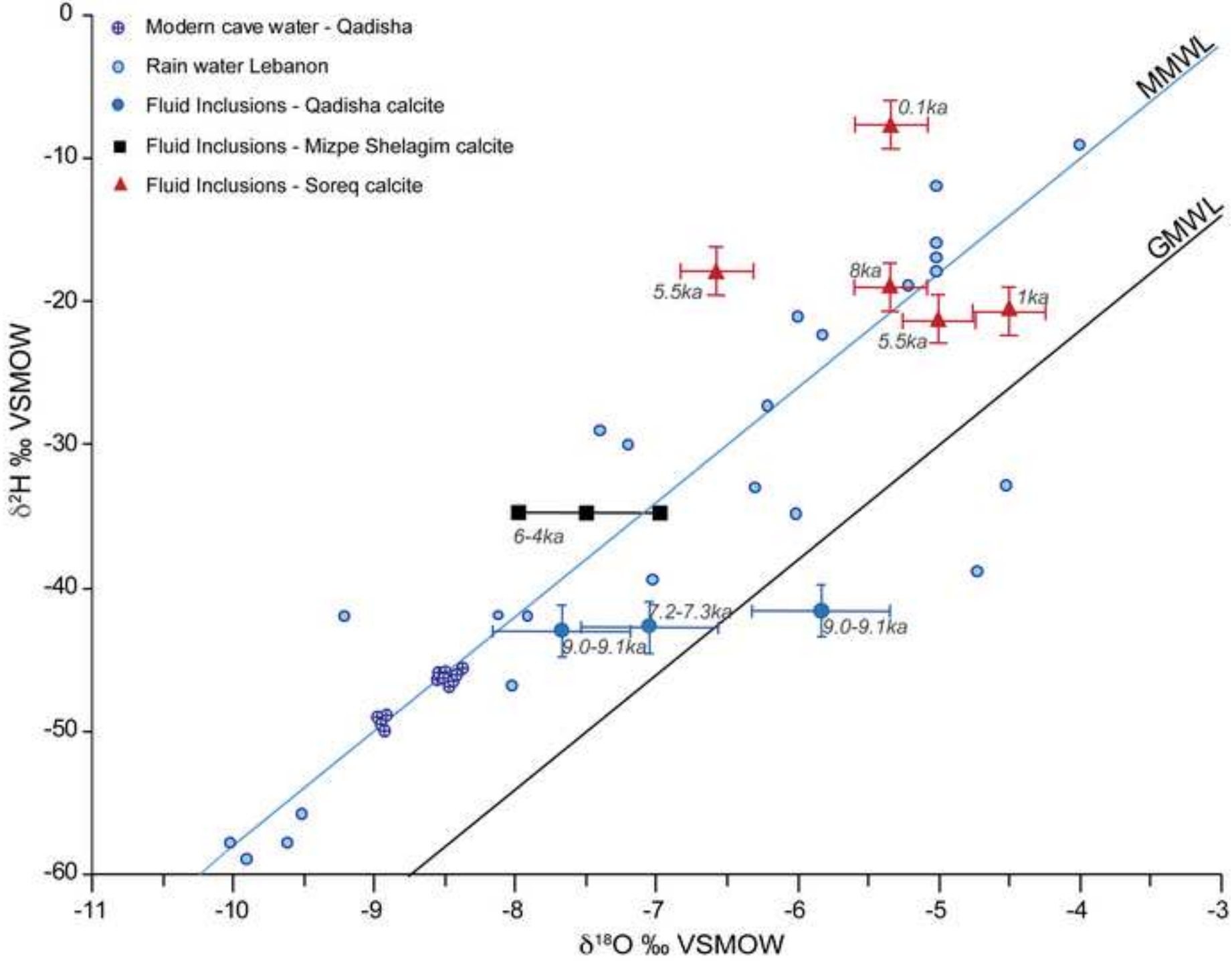

Figure 5

Click here to access/download;Figure;Fig.5_Regional SI_cave records.png

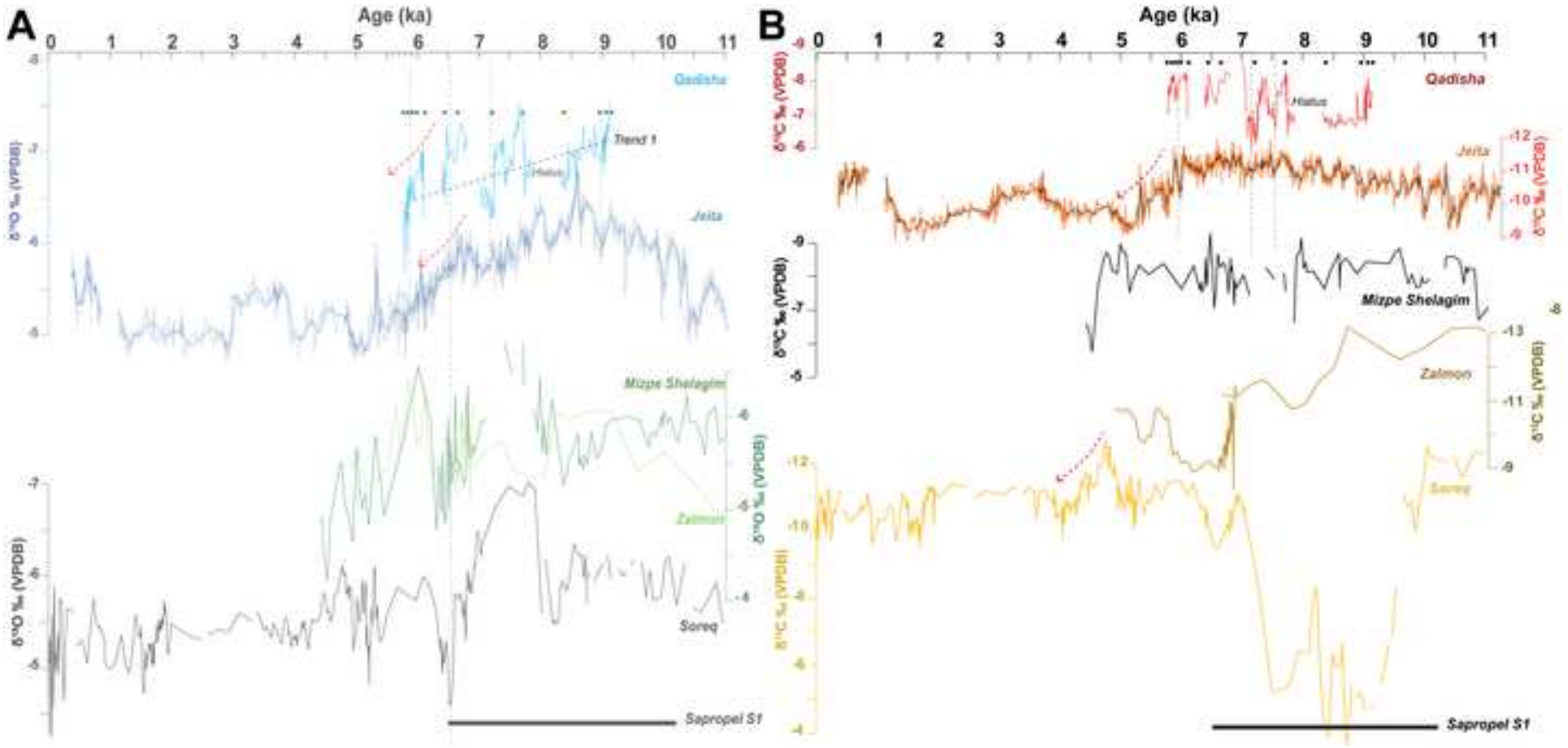

Figure 6

Click here to access/download;Figure;Fig.6_Regional_Levant_records.png

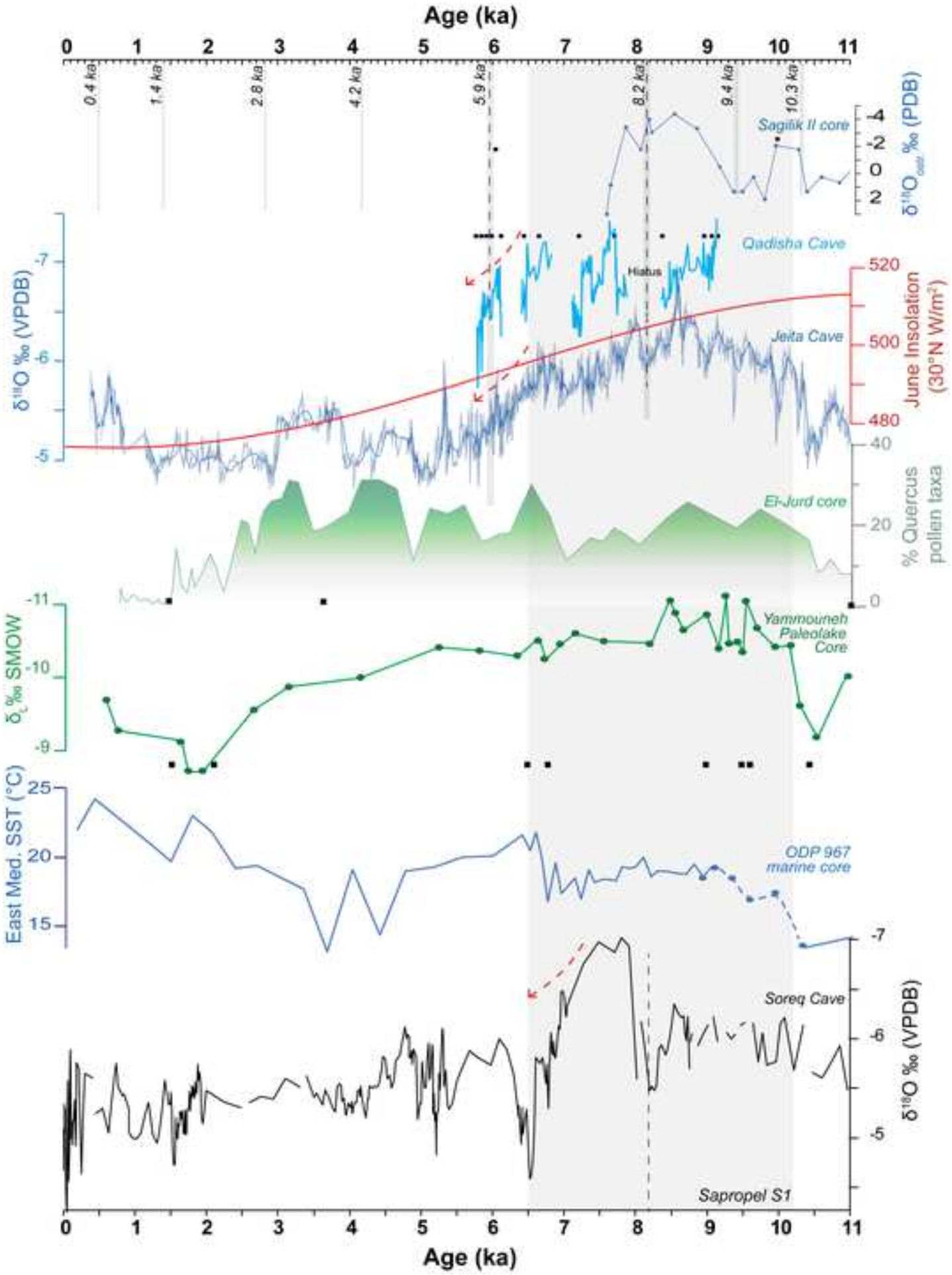

Table 1

error is 2σ error.

Sample Number	depth (mm)	^{238}U (ppb)	^{232}Th (ppt)	^{230}Th / ^{232}Th (atomic x10^{-6})	$\delta^{234}U$* (measured)	^{230}Th / ^{238}U (activity)	^{230}Th Age (a) (uncorrected)
Qad-stm1-0	2	435.0 ±1.0	3591 ±72	85 ±2	353.7 ±2.2	0.0426 ±0.0002	3848 ±19
Qad-stm1-8	7	606.5 ±0.6	132 ±3	5739 ±140	442.4 ±1.5	0.0756 ±0.0003	5853 ±28
Qad-stm1-7	26	575.7 ±0.9	97 ±3	7502 ±240	444.3 ±2.2	0.0764 ±0.0004	5914 ±30
Qad-stm1-6	46	615.3 ±1.0	122 ±3	6432 ±183	450.6 ±2.0	0.0774 ±0.0004	5966 ±29
Qad-stm1-5	65	665.4 ±0.7	361 ±8	2329 ±50	445.7 ±1.7	0.0767 ±0.0003	5929 ±24
Qad-stm1-4	77	535.7 ±1.0	466 ±10	1472 ±31	437.3 ±2.7	0.0777 ±0.0004	6045 ±33
Qad-stm1-3	96	572.6 ±0.6	352 ±7	2126 ±46	432.1 ±1.5	0.0792 ±0.0003	6185 ±28
Qad-stm1-2	101	546.2 ±0.6	66 ±2	11419 ±389	441.9 ±1.8	0.0840 ±0.0003	6528 ±25
Qad-stm1-1	115	643.7 ±1.1	1156 ±23	792 ±16	433.5 ±2.2	0.0863 ±0.0003	6748 ±28
Qad-stm1-00*	128	639.0 ±2.0	978 ±20	902 ±18	428.1 ±2.6	0.0838 ±0.0003	6573 ±24
Qad-Stm2-5	6	558.6 ±1.5	194 ±4	45 ±3	303.3 ±2.1	0.0009 ±0.0001	79 ±5
Qad-stm2-4	13	297.6 ±0.3	193 ±4	2309 ±51	397.4 ±1.7	0.0907 ±0.0004	7294 ±36
Qad-stm2-3	25	621.7 ±0.6	316 ±6	3161 ±65	406.2 ±1.4	0.0973 ±0.0002	7794 ±22
Quad 2-8.2	28.2	351.8 ±0.3	255 ±6	2284 ±50	423.4 ±1.6	0.1003 ±0.0004	7937 ±38
Qad-stm2-2	30	336.4 ±0.5	87 ±2	6980 ±178	457.5 ±2.1	0.1093 ±0.0004	8466 ±32
Qad stm2-8.6	36	367.1 ±0.3	284 ±6	2422 ±52	483.2 ±1.6	0.1138 ±0.0004	8667 ±35
Qad-stm2-8	49	499.2 ±0.7	62 ±2	15661 ±580	481.2 ±2.2	0.1186 ±0.0004	9062 ±35
Qad-stm2-7	67	582.4 ±0.8	188 ±4	6121 ±144	484.8 ±2.1	0.1200 ±0.0004	9153 ±34
Qad-stm2-6	80	566.7 ±0.8	379 ±8	2970 ±63	489.1 ±2.1	0.1206 ±0.0004	9167 ±34
Qad-Stm2-1	106	545.4 ±0.9	207 ±4	5220 ±106	472.7 ±1.4	0.1199 ±0.0002	9218 ±20

U decay constants: λ_{238} = 1.55125x10^{-10} (Jaffey et al., 1971) and λ_{234} = 2.82206x10^{-6} (Cheng e

*$\delta^{234}U = ([^{234}U/^{238}U]_{activity} - 1)$x1000. ** $\delta^{234}U_{initial}$ was calculated based on ^{230}Th age (T), i.e., $\delta^{234}U_{initia}$

Corrected ^{230}Th ages assume the initial $^{230}Th/^{232}Th$ atomic ratio of 4.4 ±2.2 x10^{-6}. Those are the values equilibrium, with the bulk earth $^{232}Th/^{238}U$ value of 3.8. The errors are arbitrarily assumed to be 50%.

***CE stands for "Contemporeneous Era". Ages are defined as the year before 1950 A.D.

* age considered as outlier

^{230}Th Age (a) (corrected)	$\delta^{234}U_{Initial}$** (corrected)	230Th Age (yr CE)*** (corrected)
3307 ±127	357 ±2	**3247 ±127**
5848 ±28	450 ±1	**5780 ±28**
5911 ±30	452 ±2	**5843 ±30**
5962 ±29	458 ±2	**5894 ±29**
5918 ±25	453 ±2	**5850 ±25**
6028 ±35	445 ±3	**5960 ±35**
6173 ±29	440 ±2	**6105 ±29**
6525 ±25	450 ±2	**6457 ±25**
6711 ±38	442 ±2	**6643 ±38**
6542 ±32	436 ±3	**6482 ±32**
71 ±7	303 ±2	**5 ±7**
7281 ±37	406 ±2	**7213 ±37**
7783 ±23	415 ±1	**7715 ±23**
7922 ±39	433 ±2	**7851 ±39**
8461 ±33	469 ±2	**8393 ±33**
8652 ±36	495 ±2	**8581 ±36**
9060 ±35	494 ±2	**8992 ±35**
9147 ±34	497 ±2	**9079 ±34**
9154 ±35	502 ±2	**9086 ±35**
9211 ±21	485 ±1	**9145 ±21**

t al., 2013). Th decay constant: $\lambda_{230} = 9.1705 \times 10^{-6}$ (Cheng et al., 2013).

$_{l} = \delta^{234}U_{measured} \times e^{\lambda_{234} \times T}$.

for a material at secular

Table 2

Qad_2 FI	Age of level [ka CE]	Sample code	**δ**H2 [permil]	**δ**18O [permil]	Volume [µl]	Mass [g]	Water amount [µl/g]	T_{fi} [°C]
Level B	9.0-9.1	BQ_2_d	-41.70	-5.81	0.29	0.58	0.50	18.7±2.5
Level B	9.0-9.1	BQ_2_b	-43.20	-7.65	0.73	0.78	0.94	10.3±2.5
Level B*	9.0-9.1	BQ_2_a	-39.58	-5.53	0.23	0.72	0.32	20.1±2.5
Level A	7.2-7.3	AQ_1	-42.82	-7.04	0.39	0.46	0.84	12.2±2.3
Level E*	0.05	EQ_1	-19.46	-6.88	0.01	0.45	0.02	11.2±2.4

This piece of the submission is being sent via mail.